Calibration of the MINERvA Test Beam and Verification of Medium Energy Geometries

A thesis submitted in partial fulfillment of the requirement
for the degree of Bachelor of Arts / Science in Department from
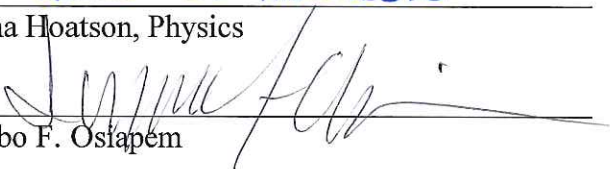The College of William and Mary

by

Cora Karamitsos

Accepted for _____ HONORS _____
(Honors or no-Honors)

_____
Jeff Nelson, Director

_____
Gina Hoatson, Physics

_____
Iyabo F. Osiapem

Williamsburg, VA
April 28, 2015

Verification of Medium Energy Geometries & Calibration of the Test Beam

Cora Karamitsos

Physics Department

College of William and Mary

Williamsburg, VA

April 20, 2015

Abstract

The MINERvA experiment studies neutrino-nucleus interactions using muon neutrinos and antineutrinos. MINERvA is specifically designed to obtain information on neutrino cross sections. At Fermi National Accelerator Laboratory (Fermilab) a beam of 120 GeV protons hits a one meter long graphite target to produce pions and kaons that decay to produce neutrinos. Because neutrinos are electronically neutral particles, they do not strongly interact with matter. When they do interact, they can only be detected though the secondary particles produced in that interaction. Therefore the MINERvA detector relies heavily on information about the properties of particles like pions, protons, electrons and kaons of different momentum. A small version of the MINERvA detector was constructed to imitate the large MINERvA detector and provide a calibration for the energy scale of calorimetric reconstruction. Therefore it is important to use a well understood beam of hadrons to accurately calibrate the main detector. This beam is produced at the Fermilab Test Beam Facility (FTBF). The test beam used for these calibrations was a momentum selected beam of pions, electrons, protons and kaons. I worked on data analysis for the Time of Flight (ToF) system, which used the time it takes for a particle of known momentum to traverse a known distance to identify that particle.

Introduction

The purpose the MINERvA experiment is to study neutrino and anti-neutrino interactions for a variety of nuclei. The MINERvA experiment is designed to attain measurements of neutrino cross sections with unprecedented precision. Cross sections describe the probability that different types of interactions will occur. Previous experiments have made precision measurements of these cross sections of neutrinos with high energy, greater than 15 GeV, but there is not precise data for the cross sections of neutrinos with energies of 3 to 6 GeV. MINERvA's use of the Neutrinos in the Main Injector (NuMI) beam focuses on these energy ranges. The cross sections measured by MINERvA will enable future experiments, like NOvA, to search for differences between the neutrino and the anti-neutrino oscillation and potentially explain why we live in a matter-dominated Universe.

Description of the Medium Energy NuMI Beam

At Fermilab, protons are accelerated to 120 GeV within the Main Injector and then directed towards the underground target hall. The protons are not a continuous beam but short 10 μs spills, which occur about every two seconds. The average beam power is about 350 kilowatts. The instantaneous power of the beam is actually significantly larger within each spill.

The beam of protons then pass through a collimating baffle which removes the wide tails of the beam. The baffle also acts to protect the target and horns from stray protons. Then the beam is steered into a graphite target that is approximately one meter long. This length corresponds to two nuclear interaction lengths. An interaction length is the mean path length required to reduce the numbers of relativistic charged particles by a factor of 1/e. This length changes depending on the particles in the beam, the energy, and the material of the target. The target is narrow, with a width of about 7.4 cm. This allows for secondary particles to easily exit. The interaction of protons with carbon produces many different particles. The target is not a single piece of graphite, but instead is composed of multiple fins. Each fin is the same shape and dimension and is evenly spaced, with the exception of

$$pC \to \pi^{\pm}X \qquad \begin{array}{l} \pi^+ \to \mu^+ + \nu_\mu \\ \pi^- \to \mu^- + \bar{\nu}_\mu \end{array} \qquad \begin{array}{l} K^{\pm} \to \mu + \nu_\mu \\ K^0_L \to \pi + \mu + \nu_\mu \end{array}$$
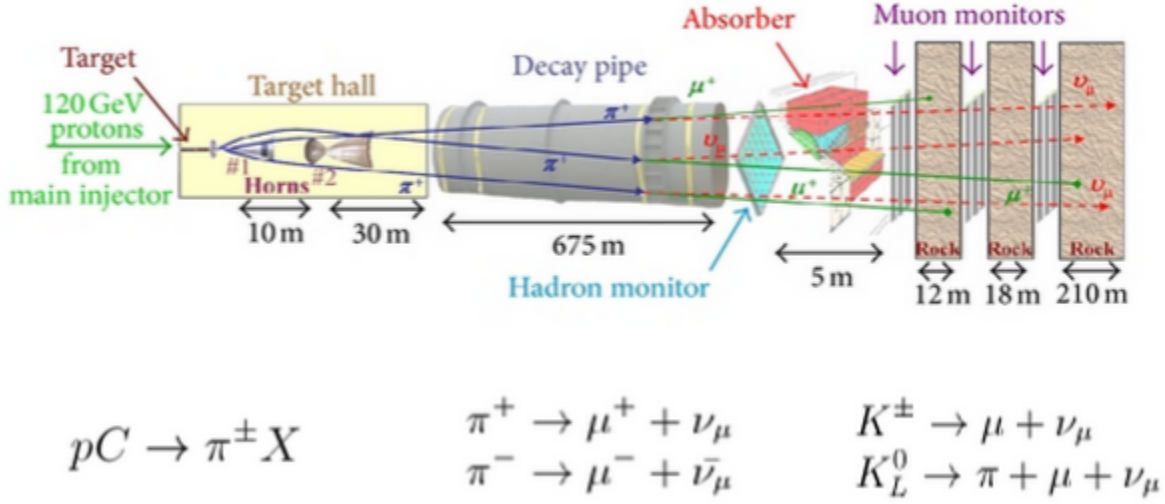
Figure 1: Target Hall Setup and Interaction Equations.

the budal monitor and the first fin. The budal monitor is used to position the beam on the target.

Both charged kaons and charged are focused with magnetic horns. These cylindrically symmetric horns are depicted in Figure 2. The blue region contains a magnetic field. This field is created by running 185,000 amps through the inner and outer surfaces of the conductor of the horns. A change in direction of the current can focus either positive or negative particles, effectively creating a beam of either neutrinos or antineutrinos. These horns are also moveable and by changing their position, relative to the other volumes, pions and kaons of specific energy ranges can be focused.

After being focused by these magnetic horns the beam of pions and kaons pass into a decay pipe which is filled with helium. Helium has a light nucleus and is used in the decay pipe to reduce particle interactions. The decay pipe is 675 meters long and by the time the beam exits the decay pipe, most of the pions and kaons have decayed, producing either neutrinos or antineutrinos and charged leptons. Following the decay pipe the beam passes through a hadron monitor and a hadronic absorber. These two apparatuses are meant to take data on the flux and energy of the remanent hadrons and also absorb them. Then the beam
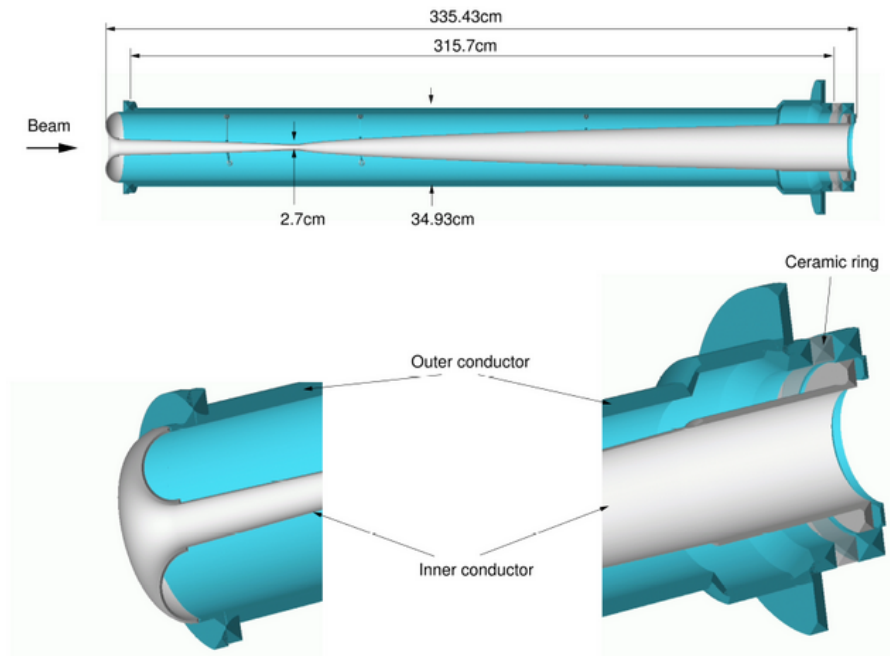
2

Figure 2: Horn One uses electric current flowing through the outer conductor to create a cylindrically symmetrical magnetic field. This magnetic field focuses off axis particles in the beam.

passes through three muon monitors which have expanses of rock in between. These provide data on the flux of muons as well as absorb the muons. Taking data on the flux of muons is valuable because most decays that produce neutrinos also produce muons. Therefore the flux of muons is a good approximation of the flux of neutrinos and useful in understanding the NuMI beam.
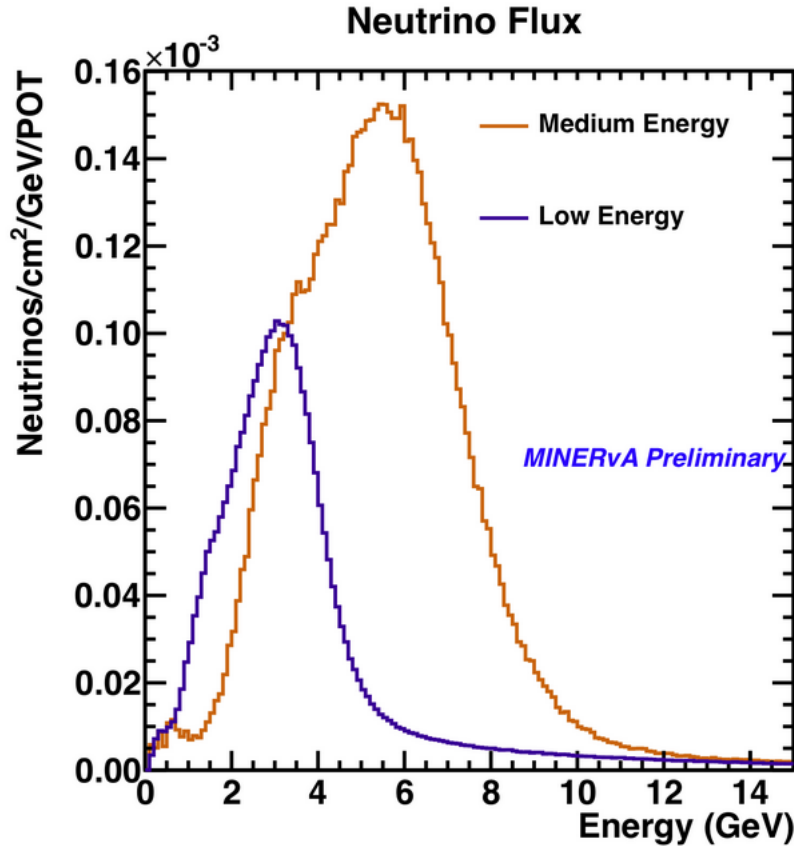
Figure 3: Flux of Neutrinos as a function of Beam Energy for Medium Beam Energy.

After creating this beam of neutrinos the beam passes through the MINERvA detector. The same beam is used in NOvA and MINOS. The beam used for MINERvA's experiments has recently shifted from the Low Energy beam (LE), peaking at 3 GeV, to the Medium Energy beam (ME), which peaks at around 7 GeV. Figure 3 shows the number of neutrino events versus the energy of neutrinos for the medium energy beam. This change is due to

4

the NOvA experiment changing beam energies, and MINERvA is a parasitic experiment that uses the same beam line. Multiple experiments can be used on the same beam of neutrinos because neutrinos are weakly interacting particles and most pass through hundreds of kilometers of material without interacting. This change in beam energy has necessitated a change in the beam configuration. A new target has been employed and the relative distances of the horns have been changed. The new distances are reflected in Figure 1.

GEANT4 and HepRApp

GEANT4 is a computer program that simulates particle interactions. It contains cross sections for different particles at different energies and branching ratios that describe what the result of the interaction will be. These cross sections and branching ratios come from data collected by experiments and is not always completely accurate. There are different options within GEANT4 that focus on different types of simulation. Since the change from LE to ME GEANT4 has been updated to simulate the beam production. The program that uses GEANT4 to model the beam production is called g4numi.

HepRApp is a visualization tool that I used to view the volumes in the virtual geomety within the g4numi code. HepRApp uses the same nomenclature as g4numi and I was able to become familiar with the relative locations of each volume. In this program the volumes were divided into subdivisions. There were variables that encompassed the entire target hall. Each horn was subdivided into an inner conductor, outer conductor, front and end piece. There are also theoretical volumes in HepRApp that don't correlate with physical volumes but define a space where a volume of empty space. HepRApp also makes approximations in the visualization of certain volumes; for example complicated curvatures are sometimes left out of the visualization.

Verification of Medium Energy Geometries for MINERvA Beam Production

Because the g4numi Monte Carlo calculator yielded a significantly different energy peak in the flux of neutrinos than what was actually observed, Mike Kordosky, a William and Mary professor who works on MINERvA, started to investigate the code using HepRApp. He found that g4numi included an extra graphite fin in the target and this led him to suspect that there were other inconsistencies in g4numi. I investigated whether other aspects of the g4numi code were correct.

I started by confirming that the target was correct and verified the dimensions of the fins. The actual carbon fins have a cylindrical curvature on either side that was not included in HepRApp but is assumed to be apparent in the actual g4numi code. If the half cylinders on each target fin is added to the HepRApp representation of the fins, then the spacing between the fins is correct. I also checked the fin spacing between the budal monitor and the first fin and the spacing between the first fin and the second fin. I then checked the relative distances of the target to the first horn. I confirmed that these all seemed to be correct and consistent with engineering drawings. I found in NuMI documentation that the distance between MCZERO and ACTRN2 should be 19180.0 mm but in HepRApp I found the distance from the front of horn 1 to the front of horn 2 to be 18983.5 mm. The second horn in the simulation should be farther back than it is. However, moving the horn back farther would actually move the simulation's peak energy for the neutrinos even higher and would only have about a 1% effect. Therefore while I confirmed this relative distance to be incorrect in the g4numi simulation, it does not account for the discrepancy between the Monte Carlo and what is observed. I concluded that I could not identify a discrepancy in the g4numi geometries that could account for the difference in the Monte Carlo calculator and observation.

MINERνA Detector

The MINERvA detector is designed to accurately measure neutrino-nucleon cross sections. Because neutrinos are neutral particles and do not interact strongly in matter, in order to study the interaction of a neutrino on a nucleus, it is necessary to reconstruct event given information about the secondary particles. Scintillator is used to track the trajectory and energy deposits of secondary particles. Fiber optics within each scintillator strip are connected to photomultiplier tubes (PMTs), who's signals are then digitalized and read out through a Data Acquisition (DAQ) system, and stored to a disk.
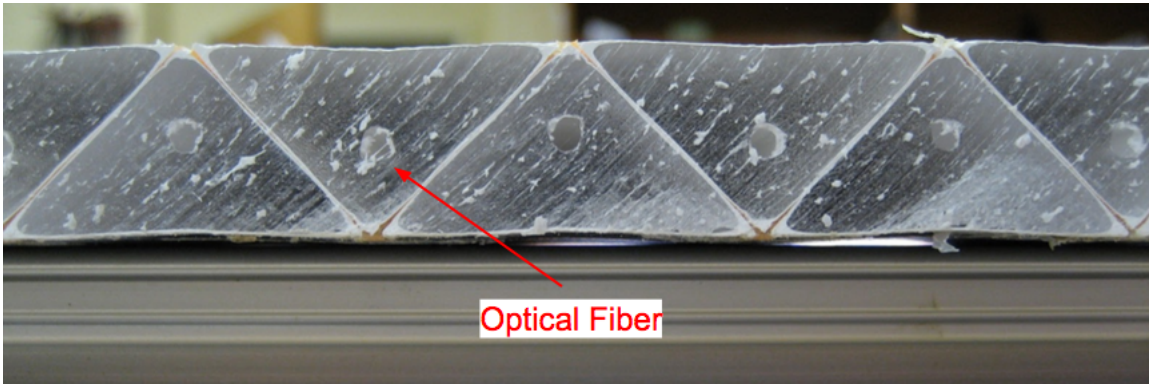
Figure 4: Side View of Scintillator Strips in a plane.

Triangular strips of scintillator are stacked together to create a plane. Because of the diagonal sides of each of the strips adjacent to one another, most particles passing through a plane pass through two scintillator strips at a time. The proportion of light deposited in the two scintillator strips allows for an accurate reconstruction of the location of the particle when it passed through. Each plane is covered in black plastic to prevent the leakage of light. These scintillator planes are dispersed throughout the detector.

The MINERvA detector utilizes both electromagnetic calorimetry and hadronic calorimetry. The active tracker region, as seen in Figure 5, is completely scintillator and meant to track the secondary particles that interact with the various nuclear targets. The nuclear targets include liquid helium (He), carbon (C), lead (Pb), iron (Fe), and water (H_2O). The Electromagnetic Calorimeter (ECAL) uses lead sheets to slow high energy particles and
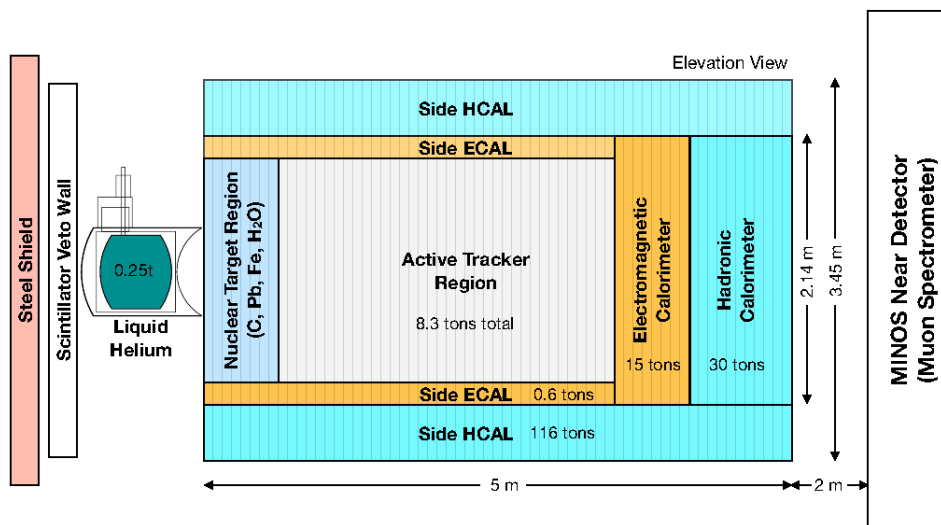
Figure 5: MINERvA Detector Side View.

create a spray of low energy particles from the secondary particles. Hadronic Calorimeter (HCAL) is used to slow particles that interact via the strong nuclear force. The MINERvA HCAL system uses steel plates and scintillator to contain secondary particles from hadronic interactions. Both calorimetric systems are used to slow or stop particles so that their energy can be measured more accurately. The MINERvA is composed of over 200 planes in total.
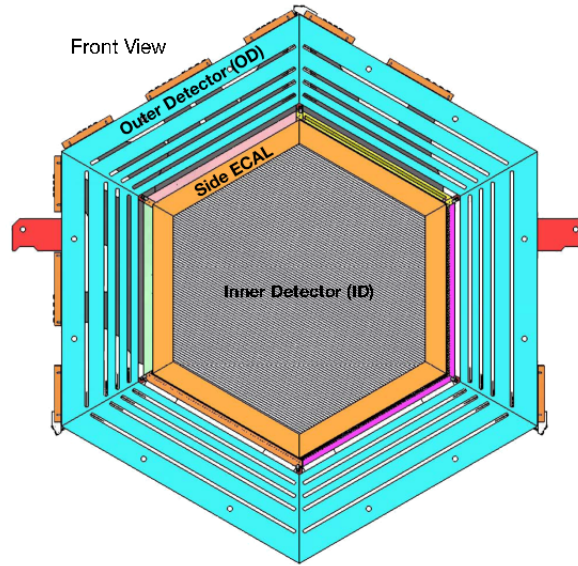

Figure 6: MINERvA Detector Frontal View.

Test Beam

The purpose of the test beam is to send particles of known momentum through a detector in order to calibrate the measurements of the detector. We will use a secondary beam of pions, electrons and protons that is generated by a beam of 120 GeV protons. A similar experiment was run in 2010 in order to calibrate MINERvA's measurements and found the overall uncertainty to be 4% for pions and 3% for protons and electrons. However the beam used in 2010 was a tertiary beam of energy 400 MeV to 1,800 MeV. The momentum of the secondary beam is 2 GeV to 20 GeV and is a better match for the secondary particles produce in ME neutrino interactions. The goal of this project is to better understand this

9

beam.

The test beam is produced when 120 GeV protons interact with a carbon target. The secondary particles are bent in a magnetic field and pass through a collimator. The collimator allows for the selection of secondary particles of a 2% band of momentum. The beam then passes through the Time of Flight (ToF) system, 4 tracking multi-wire drive chambers and the Cherenkov detector before arriving at the Test Beam Detector (Aliaga).

Test Beam Detector

The detector can be modified to imitate the different actual detector components used by MINERvA. The detector allows different materials to be slid in between the scintillator planes. This run will be comprised of three different configurations. The first configuration has 20 ECAL and 20 HCAL planes. ECAL planes are composed of scintillator and 2mm lead. The second configuration is meant to test our simulations secondary particle leakage out the back of the MINERvA detector. The HCAL planes are composed of scintillator planes and one inch of iron. The last configuration has 20 layers of tracker and 20 ECAL planes. Tracker planes are just scintillator. These different configurations simulate the three different main components of the MINERvA detector. The test runs started with the ECAL/HCAL configuration and moved onto the thick HCAL configuration at the time of this thesis.

Time of Flight System

The Time of Flight (ToF) system is used in order to identify particles of known momentum. The ToF system in the test beam consists of two scintillator paddles, one in the early beam line and one immediately in front of the test beam detector. Because the distance between the two ToF paddles and the momentum of the particles is well known, the mass of the particle can be determined using the following equations, where c is the speed of light and t is the time of flight.

$$\beta = \frac{v}{c} \tag{1}$$

$$p = \gamma m v \tag{2}$$

$$\gamma = \frac{1}{\sqrt{1 - \beta^2}} \tag{3}$$

$$v = c\sqrt{\frac{p^2}{p^2 + m^2}} \tag{4}$$

$$t = \frac{distance}{v} \tag{5}$$

Cosmic Detectors

The Test Beam system includes cosmic ray detectors that allow for the Test Beam Detector to be triggered by the passage of cosmic ray muons. Muons deposit approximately the same amount fraction of their energy in each scintillator strip that they pass through. Because cosmic ray muons are such high energy, this fractional energy deposit is approximately equal in each scintillator strip. Therefore a cosmic muon passing through the detector allows for the calibration of each individual scintillator strip that the muon passes through.

Veto System

The Veto System is used in order to increase the efficiency of the test beam detector. The Veto System looks for multi-particle events from the beam and excludes the events that do not go through both wire chambers from the DAQ. In order to exclude this data from the test beam DAQ there is an array of scintillator paddles with a rectangular gap in front of the detector. Only the particles that make it through this gap and do not trigger the Veto System are recorded as data.

Fermilab Test Beam Shifts

During winter break I travelled to Fermilab, outside of Chicago. This is where the MINERvA experiment is based. The intention of the trip was to monitor runs of the Test Beam

experiment in shifts. However because of technical difficulties in implementing the Data Acquisition (DAQ) system, the Test Beam was not fully operational. I spent time working to calibrate the Veto System as part of the Test Beam commissioning. I also did a shadow shift of the MINERvA Main Detector and ran tests to calibrate the scintillator paddles in the Veto System.

Time of Flight Calibration and Analysis

My analysis looks at the data from the Time of Flight system and quantifies the errors associated with the particle composition of the beam at different momenta. The goal was also to determine the intrinsic resolution of the beam line. There are various physical volumes that the test beam passes through before reaching the test beam detector. The particles in the beam have the potential to interact within these volumes. There is also a momentum spread in the beam line. Both of these factors contribute to an error in the momentum of the particles going through the detector. By analyzing the time of flight data I was able to quantify these errors.

Trigger of the Time of Flight System

The ToF system will only collect data if it is triggered to do so. The trigger system will fire when a coincident signal from three scintillator paddles in the beam line as well as a signal indicating that the beam spill is occurring. After receiving a trigger the DAQ is opened for 125 ns. The trigger system is important so that two separate particles don't signal the ToF paddles separately and yield spurious triggers. In practice this a perfect system. Later in the Results section I will show that there is a periodic spill of particles in the ToF data at every 19 ns, which is the spacing within the spill structure of the 120 GeV proton beam.

Multiple Scattering through Small Angles

Charged particles traveling through mediums are deflected by many small angles as they travel. The majority of this scattering is due to the Coulomb force. For small deflections

this scattering is roughly Gaussian. Given the following equation it is possible to calculate the degree of scattering as charged particles pass through matter (Bichsel). Using this equation I worked through the maximum angle of defection given different materials of different widths. The results of my calculations can be seen on table 1. The charge number for all particles considered is 1.

Variable	Definition
θ_0	is the angle of deflection
p	is the momentum
βc	is the velocity
z	is the charge number of incident particle
$\frac{x}{X_0}$	is the thickness of the scattering medium in radiation lengths

$$\theta_0 = \frac{13.6 MeV}{\beta cp} z \sqrt{x/X_0}[1 + 0.038 ln(x/X_0)] \tag{6}$$

Table 1: Multiple Scattering Through Small Angles

Material	$\frac{x}{X_0}$	Momentum (p)	Particle	Velocity (βc)	Angle of Deflection (θ_0) Radians
Scintillator	42.2	2 GeV	Electron	0.99999996c	$1.682*10^{-10}$
			Pion	0.99757c	$1.686*10^{-10}$
			Proton	0.90537c	$1.858*10^{-10}$
Lead	0.56	4 GeV	Electron	0.999999991c	$8.294*10^{-12}$
			Pion	0.999391c	$8.299*10^{-12}$
			Proton	0.97358c	$8.519*10^{-12}$
Helium	756	6 GeV	Electron	0.999999996	$2.6006*10^{-10}$
			Pion	0.999729c	$2.6013*10^{-10}$
			Proton	0.987999c	$2.6322*10^{-10}$

Cherenkov Radiation

Because light travels more slowly through media than in a vacuum, it is possible for a particle to move faster than the speed of light in a medium. Cherenkov radiation is the electromagnetic radiation that is emitted when a charged particle passes through a dielectric medium at a speed greater than the phase velocity of light in that medium. A Cherenkov detector was placed in the beam line for the test beam and was triggered when an electron passed through. This pulse was recorded in the DAQ and allowed me to either suppress or select electrons in certain steps of the analysis.

Results

I analyzed the time of flight at five different momentum settings: 1.55 GeV, 2 GeV, 4 GeV, 6 GeV and 8 GeV. A run of 120 GeV protons was used to time calibrate the data from these runs so that particles traveling at the speed of light are centered around zero. Since 120 GeV protons travel close to the speed of light. After centering the data from the run around zero, I distinguished the peaks and identified the particles corresponding with each peak. I fit each peak with a gaussian in order to determine the mean value for the Time of Flight and the spread of each peak, σ, which corresponded with the error in the ToF measurement. Figure 7 depicts the ToF data for the 120 GeV protons.

Timing Resolution

The timing resolution for the Test Beam was calculated from the spread of the 120 GeV proton ToF data. This data set has a spread in the data due to the fact that when the protons pass through the ToF scintillator paddles, they do not pass through directly in the middle. There are four PMTs on the upstream counter and two PMTs for the downstream counter, all of which much receive a photon in order for the event to part of the data set. The average time of each of these PMT time readouts is taken. By fitting a gaussian to the ToF data for the 120 GeV protons I derived a timing resolution of $\sigma = 0.2319 \pm 0.0006$ ns.
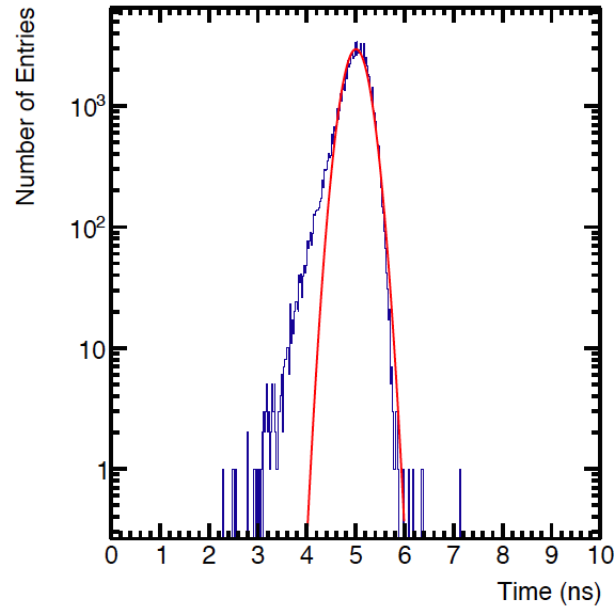
Figure 7: This plot depicts the time it took for 120 GeV protons to traverse between the two ToF scintillation paddles.

Calculated ToF compared to Measured ToF

In order to identify which peaks corresponded to which particle, I calculated the expected ToF using the momentum of the beam and the known mass of the various particles. I then compared these to the mean of each fit. The table 1 highlights my results. I used 90 meters as the distance between the two ToF paddles in order to calculate the expected ToF for each particle. After calculating these expected values I identified the corresponding peaks on the ToF data output. An example of these identifications can be seen in Figure 8.
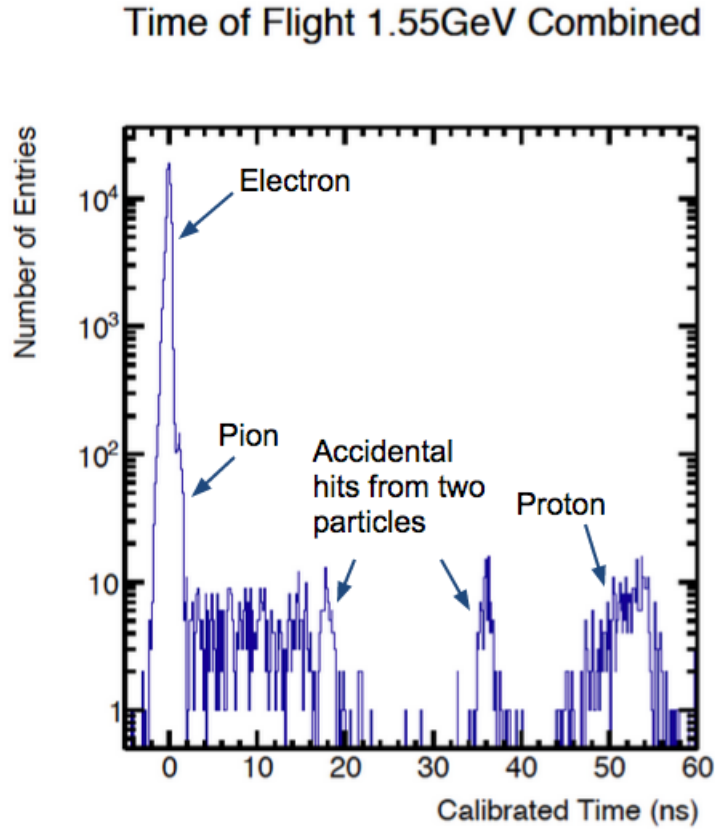
Figure 8: This plot depicts the identification of particle peaks in 1.55 GeV beam energy data.

Upstream Time 1.55GeV
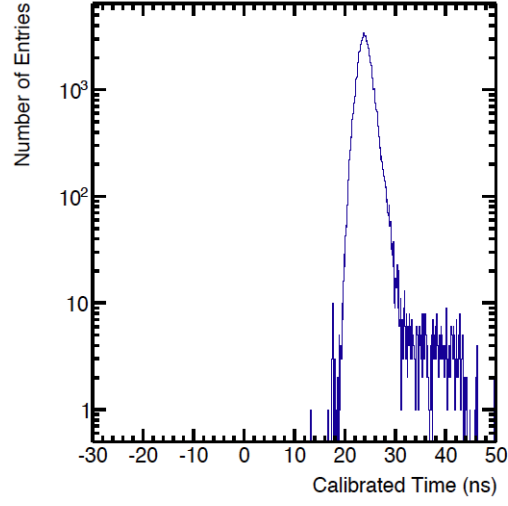
(a) This plot shows the time count recorded for the Upstream ToF Counter. The method by which the counter works is that after a hit is recorded, the counter counts until the 125 ns DAQ time period is over. this is why the upstream time stamp is greater than the downstream time stamp.

Downstream Time 1.55GeV
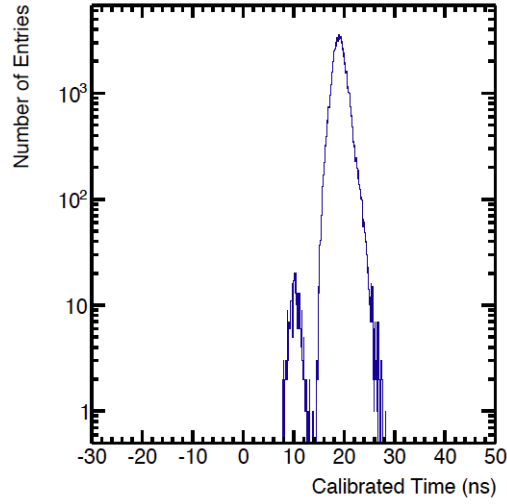
(b) This plot shows the time count recorded for the Downstream ToF Counter.

Figure 9: 1.55 GeV Upstream and Downstream Counters

17
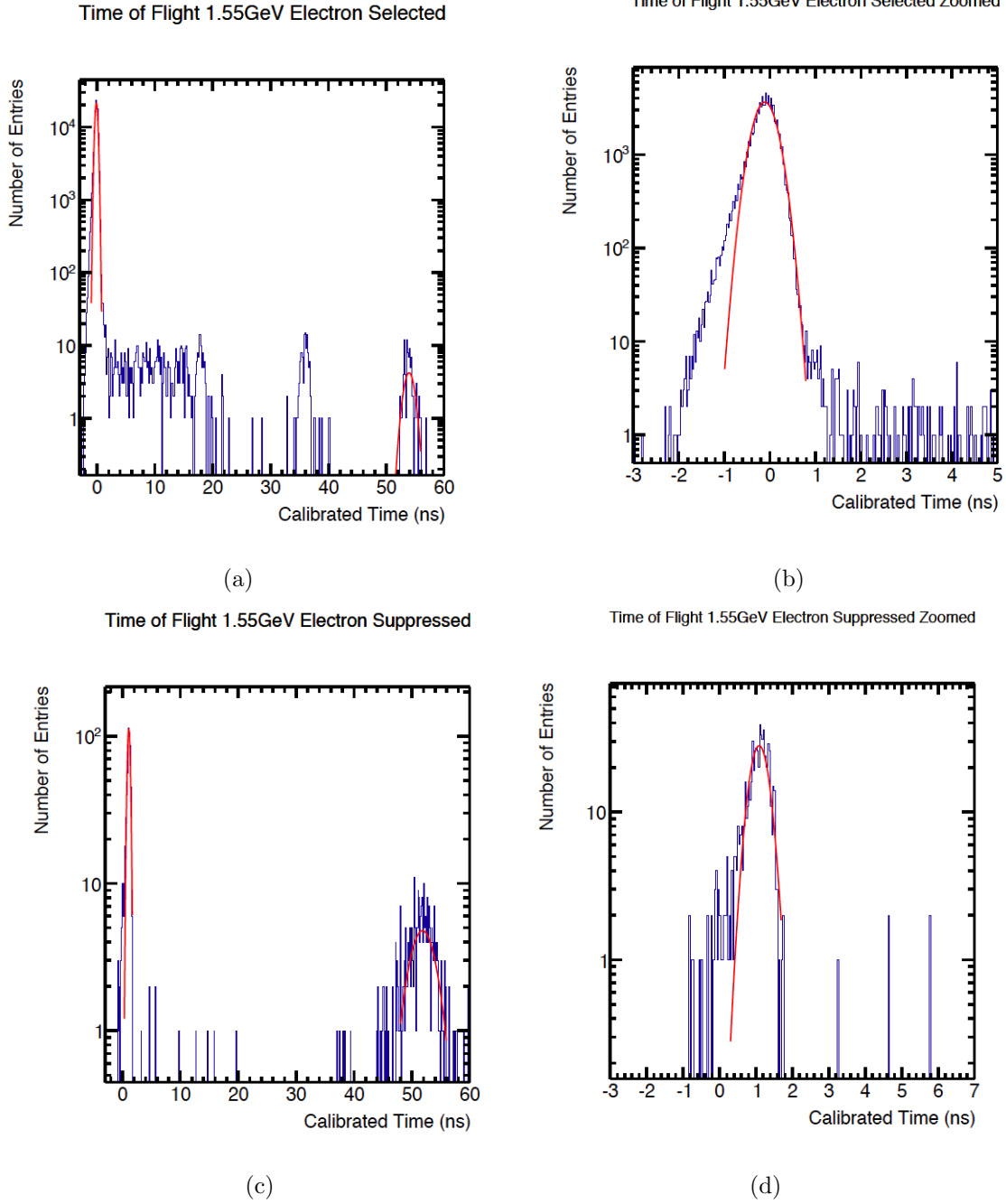
Figure 10: These plots show the 1.55 GeV ToF Data. Plots (a) and (b) show the Electron Selected data set. This is the data in which the Cherenkov Detector read out a positive signal. Ideally, this selection should only include electrons. It is clear from these plots that the majority of accidentals at this momentum are electrons. Plots (c) and (d) are the Electron Suppressed plots, in which the Cherenkov Detector read out negative. This includes pions and protons and a few remanent electrons that were not detected by the Cherenkov Detector.

18
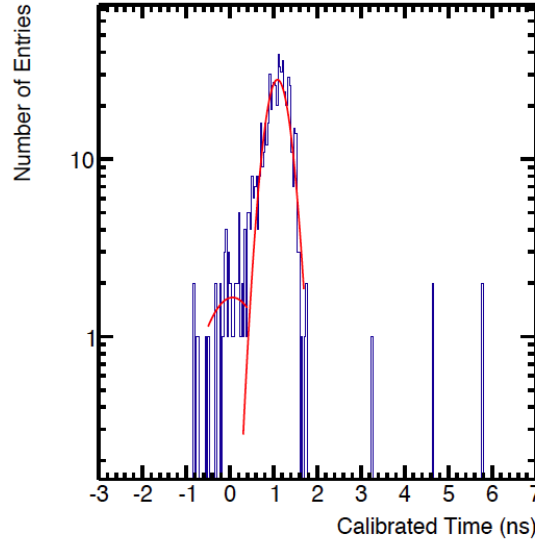
Figure 11: This plot shows 1.55 GeV Constrained Fit of the Electron Suppressed data set. The smaller peak fit on the left of the pion peak is associated with the electrons. The mean and width of the electron peak in the Electron Selected peak was applied to the fit. Although there are significantly less electrons in this sample, it is clear that electrons still contaminate this sample.

Table 2: Beam Composition 1.55 GeV

Particle	Cherenkov Selected	Number of Particles ± Error	Percent ± Percent Error
Pion	Electron Suppressed	602 ± 24.4131	0.692% ± 0.0003%
	Electron Selected	93 ± 9.64365	
Electron	Electron Suppressed	46 ± 6.78233	96.66% ± 0.003%
	Electron Selected	86947 ± 294.868	
Proton	Electron Suppressed	303 ± 17.4069	0.38% ± 0.0002%
	Electron Selected	88 ± 9.38083	

1.55 GeV Test Beam

Figure 8 shows the ToF data for the 1.55GeV beam. There are also small peaks at 18 ns and 37 ns. The pulses of protons within a beam spill occur every 19 ns and these peaks correspond particles interacting in different pulses. The peaks at 18 ns and 37 ns are seen consistently on all the ToF plots. There is a large peak at zero, which corresponds to the electrons, and a shoulder on the right which corresponds to the pion. The large peak at 50 ns corresponds to the proton peak. Because protons are significantly more massive than electrons and pions, they travel at a slower speeds at the same momentum.

Figure 9(a) and 9(b) depict the data readout for the upstream and downstream ToF counters. The upstream counter has four PMTs and the downstream counter has two PMTs. I only analyzed events that deposited light in all six of the PMTs. The time read out is not representative of "real" time due to the delays of the cables. This is why all of the time differences are calibrated to the 120 GeV proton ToF data. Figure 10(a) and 10(b) show the histogram of hits on the Time of Flight system in which the Cherenkov detector read out a negative, which is called Electron Suppressed. Ideally this plot should be devoid of all electrons, but it is possible that kaons, which would not trigger the Cherenkov detector, passed through this section of the beam line and then later decayed into electrons. It is also possible that an electron and another particle went down the beam at the same time, so that the Cherenkov did not fire, but the ToF for the electron was recorded. At this momentum there is a clear separation between the pion peak, which is centered around 1 ns, and the electron peak, which is centered around zero.

Figures 10(c) and 10(d) show the Electron Selected ToF data, in which the Cherenkov detector read out positive. There are significantly more electrons in this set of data, but the pion peak is still visible.

Figure 11 shows the constrained fit for the Electron Suppressed data set. The mean and width of the electron peak in the Electron Selected data set were saved and applied to the Electron Suppressed data. The small peak to the left of the large pion peak represents where the electrons are. It is clear that most of the electrons were removed by the Cherenkov detector from the dataset. This constraining of the electron parameters allowed for a more

accurate fit of the pion peak.

The beam composition for the 1.55 GeV Test Beam is shown in Table 2. Electron emission dominate the sample and comprise of 96.66% of the total beam. Both protons and pions comprise a fraction of a percent of the beam. There is contamination of electrons in the Electron Suppressed sample, but it is significantly smaller than the number of pions and the number of protons.

2 GeV Test Beam

Figure 12 shows the complete data set for the 2 GeV ToF Test Beam. Figure 13(a) and 13(b) show the Electron Suppressed ToF data for the 2GeV Test Beam. At this momentum there is a clear separation between the pion peak, which is centered around 1 ns, and the electron peak, which is centered around zero. However it is clear that the pion and electron peak start to merge as the momentum increases. Also, there are significantly less protons in the electron selected sample than the electron suppressed.

Figures 13(c) and 13(d) show the Electron Selected ToF data, in which the Cherenkov detector read out positive. There are significantly more electrons in this set of data, but the pion peak is still visible.

Figure 14 shows the constrained fit for the Electron Suppressed data set. Just like in the 1.55 GeV Test Beam, the small peak to the left of the large pion peak represents where the electrons are. It is clear that most of the electrons were removed by the Cherenkov detector from the dataset. This constraining of the electron parameters allowed for a more accurate fit of the pion peak.

Table 3 shows the beam composition for the 2 GeV Test Beam. Electrons still dominate the sample and comprise of 96.99% of the total beam. The protons comprise a fraction of a percent of the beam. There is contamination of electrons in the Electron Suppressed sample, but it is significantly smaller than they number of pions and the number of protons. There is a growing number of pions in the 2 GeV sample as compared to the 1.55 GeV sample.
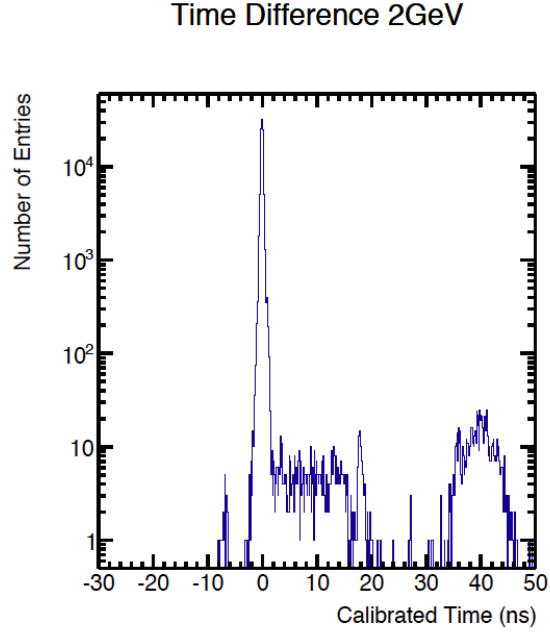
Figure 12: This plot shows the 2 GeV Total Data, which includes both Electron Selected and Electron Suppressed events. Therefore this data set includes pions, electrons and proton events.

Table 3: Beam Composition 2 GeV

Particle	Cherenkov Selected	Number of Particles ± Error	Percent ± Percent Error
Pion Peak	Electron Suppressed	1321 ± 36.3456	1.034% ± 0.006%
	Electron Selected	228 ± 15.0997	
Electron Peak	Electron Suppressed	95 ± 9.74679	96.99% ± 0.003%
	Electron Selected	123776 ± 351.818	
Proton Peak	Electron Suppressed	654 ± 27.1293	0.005124% ± 0.0002%
	Electron Selected	0 ± 1.13	
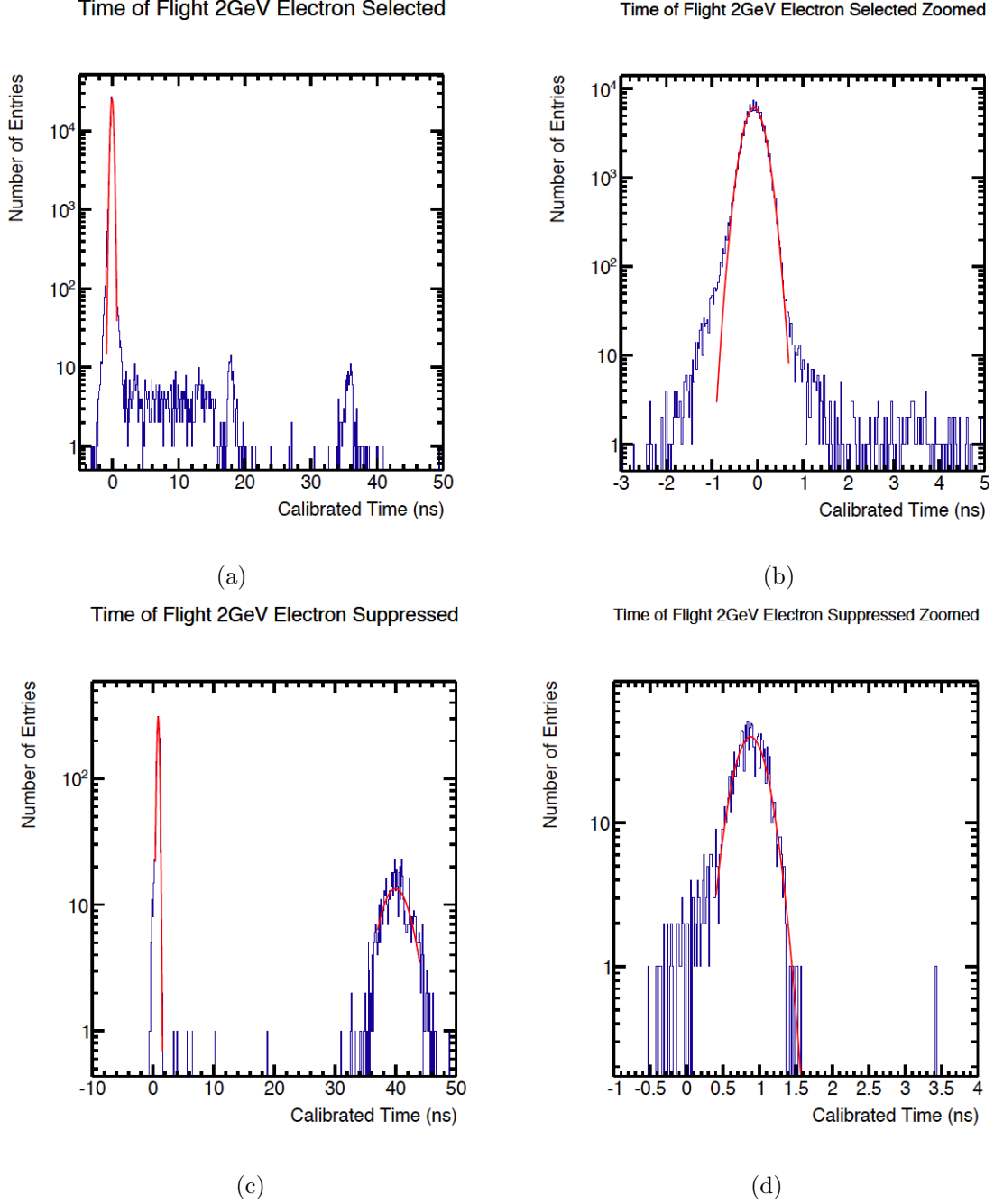
Figure 13: These plots show the 2 GeV ToF Data. Plots (a) and (b) show the Electron Selected data set. This is the data in which the Cherenkov Detector read out a positive signal. Ideally, this selection should only include electrons. It is clear from these plots that the majority of accidentals at this momentum are electrons. Plots (c) and (d) are the Electron Suppressed plots, in which the Cherenkov Detector read out negative. This includes pions and protons and a few remanent electrons that were not detected by the Cherenkov Detector.

23

Time of Flight 2GeV Electron Suppressed Constrained Fit
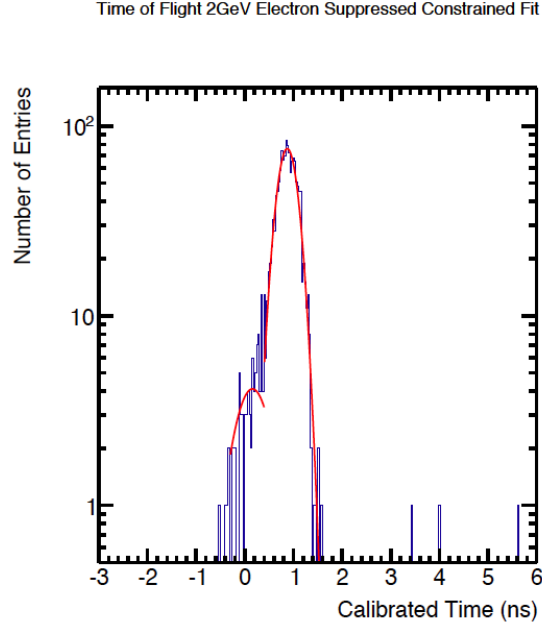
Figure 14: This plot shows 2 GeV Constrained Fit of the Electron Suppressed data set. The smaller peak fit on the left of the pion peak is associated with the electrons. The mean and width of the electron peak in the Electron Selected peak was applied to the fit. Although there are significantly less electrons in this sample, it is clear that electrons still contaminate this sample, however the electron and pion peaks are more difficult to distinguish.

4 GeV Test Beam

The ToF plots for the 4 GeV Test Beam is shown in Figure 15. The pion and electron peaks appear to be indistinguishable at this beam momentum. Therefore the average efficiency of the Cherenkov detector, which was calculated to be $6.96 \times 10^{-4} \pm 0.84 \times 10^{-4}$, was used to estimate the number of pions in the Electron Selected peak and the number of electrons in the Electron Suppressed peak. The ToF for the 4 GeV data sets derived from the mean of the best fit gaussian were difficult to calculate accurately because of the overlap of the electron and pion peaks. There is also no evidence of a proton peak in the Electron Selected data sample.

The constrained fit for the Electron Suppressed data set is shown in Figure 16. Because the peaks are now visibly indistinguishable, the constrained fit only acts to adjust the mean of the best fit of the pion peak. The constrained fit is almost identical to the free variable fit seen in Figure 15(c). This suggests that the contamination of electrons in the Electron Suppressed data sample is very small. Further analysis of the contamination of electrons within the Electron Suppressed sample can be found in the Cherenkov Efficiency section of this paper.

Table 4 shows the beam composition for the 4 GeV Test Beam. Electrons still dominate the sample and comprise of 84.9% of the total beam. The protons comprise about 2.5% of the beam. Pions comprise 11.79% of the beam. The percent contribution of the pions and protons is increasing while the percent contribution of the electrons is decreasing as the momentum of the beam increases.

Table 4: Beam Composition 4 GeV

Particle	Cherenkov Selected	Number of Particles ± Error	Percent ± Percent Error
Pion	Electron Suppressed	21290 ± 448.2	11.794% ± 0.0025%
Electron	Electron Selected	153792 ± 392.163	84.929% ± 0.0023%
Proton	Electron Suppressed	4298 ± 93.9042	2.507% ± 0.0004%
	Electron Selected	0 ± 1.675	

Time Difference 4GeV

(a)

Time of Flight 4GeV Electron Selected

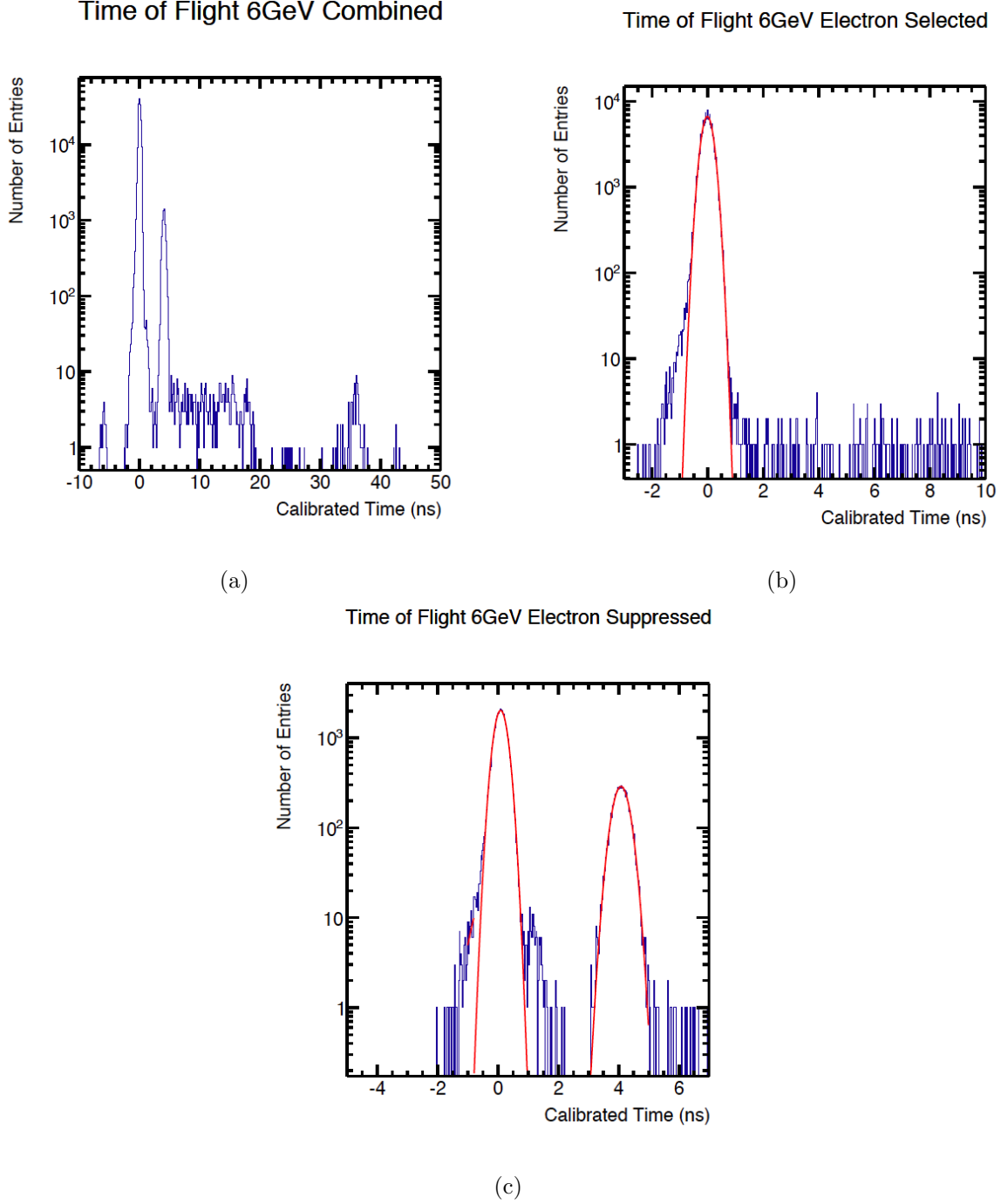(b)

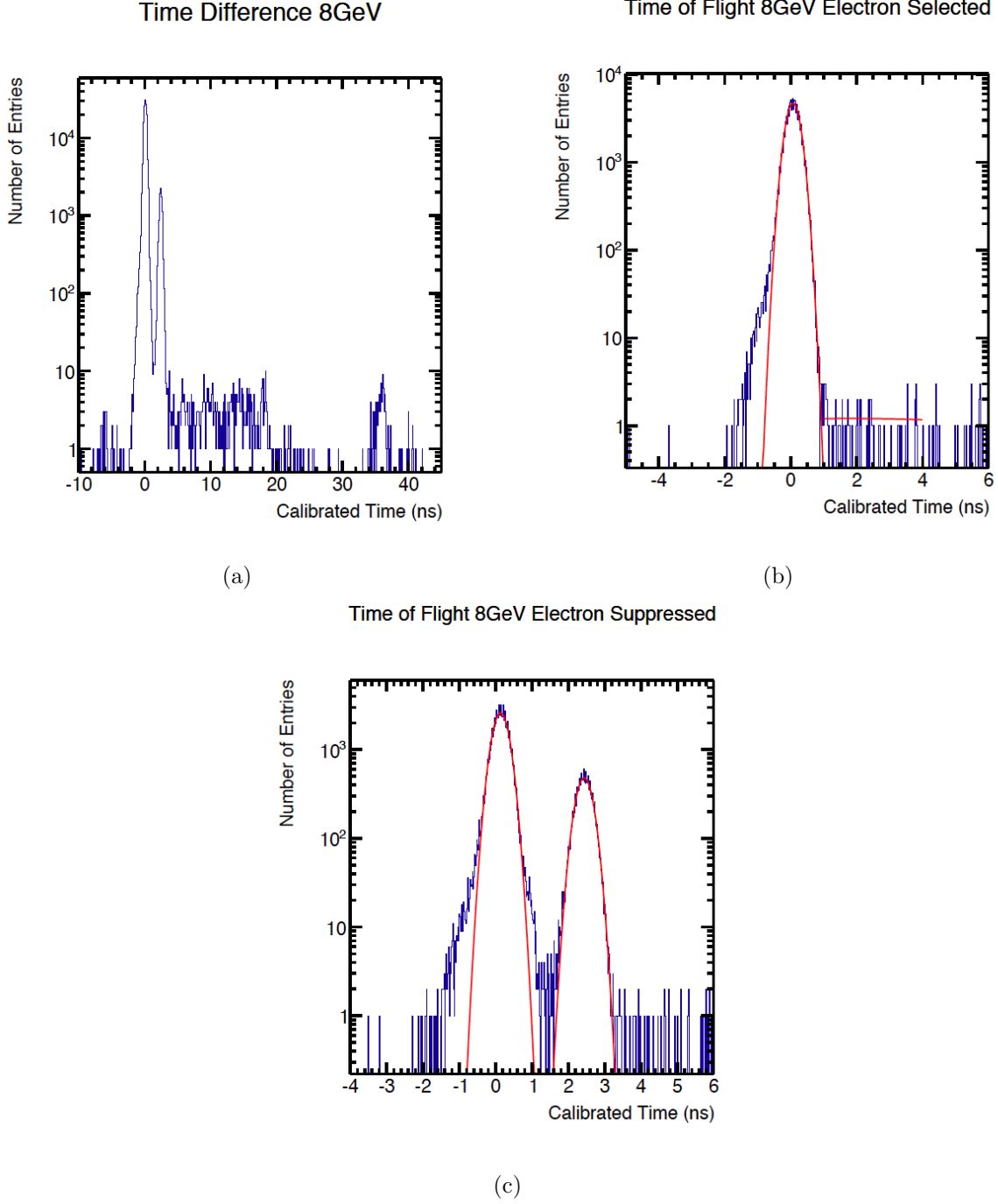**Time of Flight 4GeV Electron Suppressed**
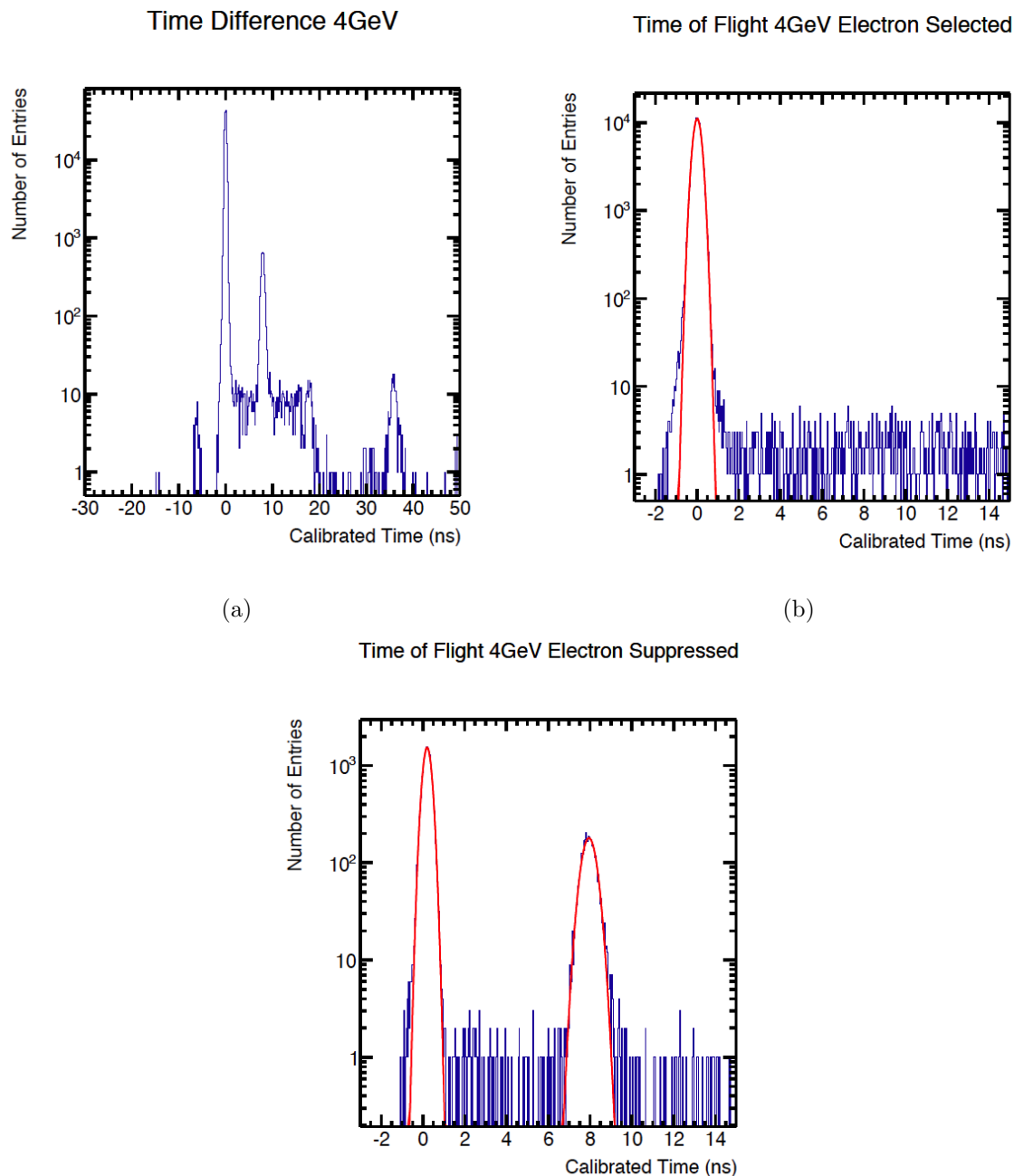
Figure 15: These plots show the 4 GeV ToF Data. Plot (a) shows the total data set, including Electron Selected and Electron Suppressed. Plot (b) shows the Electron Selected data, in which the Cherenkov Detector read out a positive signal. Plot (c) shows the Electron Suppressed plots, in which the Cherenkov Detector read out negative. This includes pions and protons and a few remanent electrons that were not detected by the Cherenkov Detector.
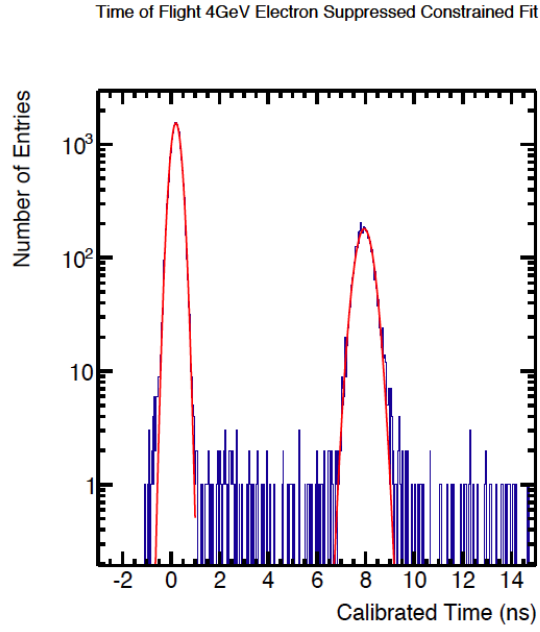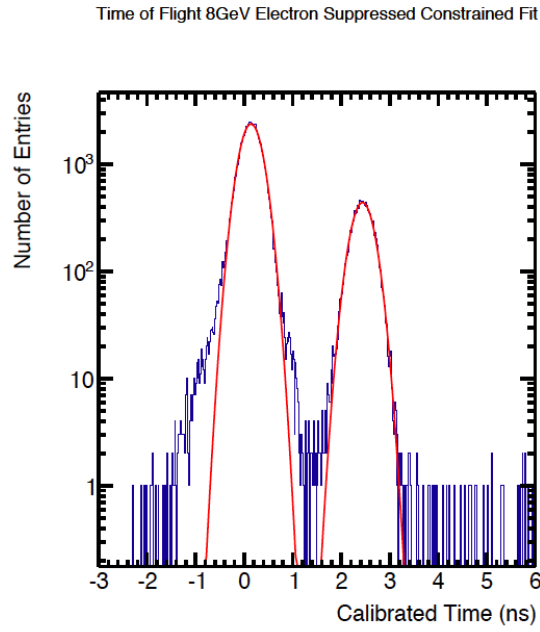
Figure 16: This plot shows 4 GeV Constrained Fit of the Electron Suppressed data set. In this data set there is no way to distinguish between the electron and pion peaks. Therefore the fits are nearly identical to the fits of the Electron Suppressed sample.

6 GeV Test Beam

The ToF plots for the 6 GeV Test Beam are shown in Figure 17. Just like in the 4 GeV Test Beam data set, the pion and electron peaks are indistinguishable at this beam momentum. Therefore the average efficiency of the Cherenkov detector was again used to estimate the number of pions in the Electron Selected peak and the number of electrons in the Electron Suppressed peak.

The constrained fit for the Electron Suppressed data set is shown in Figure 18. Again, the constrained fit is almost identical to the free variable fit seen in Figure 15(c). This suggests that the contamination of electrons in the Electron Suppressed data sample is very small.

Table 5 shows the beam composition for the 6 GeV Test Beam. Electrons still dominate the sample and comprise of 71.75% of the total beam. The protons comprise about 4.27% of the beam. Pions comprise 23.44% of the beam.

Table 5: Beam Composition 6 GeV

Particle	Cherenkov Selected	Number of Particles ± Error	Percent ± Error
Pion Peak	Electron Suppressed	43593 ± 208.789	23.443% ± 0.001%
Electron Peak	Electron Selected	133433 ±365.285	71.75% ± 0.002%
Proton Peak	Combined	7952 ± 127.295	4.27% ± 0.0007%
	Electron Selected	0 ± 1.675	

Time of Flight 6GeV Combined

(a)

Time of Flight 6GeV Electron Selected

(b)

Time of Flight 6GeV Electron Suppressed

(c)

Figure 17: These plots show the 6 GeV ToF Data. Plot (a) shows the total data set, including Electron Selected and Electron Suppressed. Plot (b) shows the Electron Selected data, in which the Cherenkov Detector read out a positive signal. Plot (c) shows the Electron Suppressed plots, in which the Cherenkov Detector read out negative. This includes pions and protons and a few remanent electrons that were not detected by the Cherenkov Detector.

29
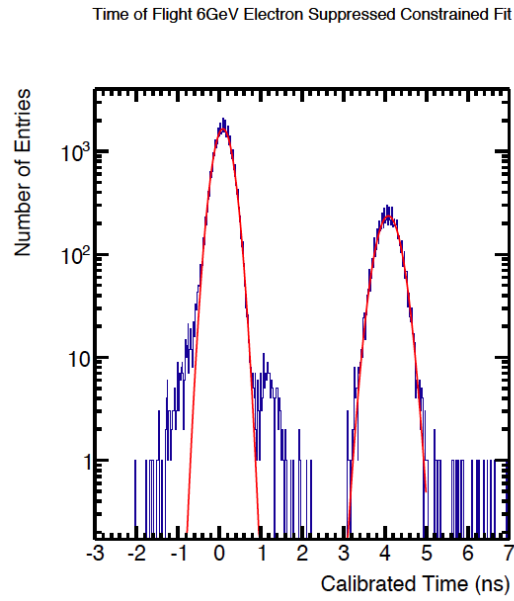
Figure 18: This plot shows 6 GeV Constrained Fit of the Electron Suppressed data set. In this data set there is no way to distinguish between the electron and pion peaks. Therefore the fits are nearly identical to the fits of the Electron Suppressed sample.

8 GeV Test Beam

Much of the same analysis from the 6 GeV Test Beam is applicable to the 8 GeV Test Beam. The same method of using the Cherenkov efficiency to calculate the number of pions and electrons in both the Electron Selected and Electron Suppressed samples was used.

Table 6 shows the beam composition for the 8 GeV Test Beam. Electrons still dominate the sample and comprise of 56.63% of the total beam. The protons comprise about 6.71% of the beam. Pions comprise 35.19% of the beam. The percent contribution of the pions and protons is increasing while the percent contribution of the electrons is decreasing as the momentum of the beam increases.

Table 6: Beam Composition 8 GeV

Particle	Cherenkov Selected	Number of Particles $\pm$ Error	Percent $\pm$ Error
Pion Peak	Electron Suppressed	71136 ± 266.713	$35.188\% \pm 0.0016\%$
Electron Peak	Electron Selected	114477 ± 338.344	$56.627\% \pm 0.0013\%$
Proton Peak	Combined	13588 ± 116.568	$6.71\% \pm 0.0006\%$
	Electron Selected	0 ± 2.534	

Figure 19: These plots show the 8 GeV ToF Data. Plot (a) shows the total data set, including Electron Selected and Electron Suppressed. Plot (b) shows the Electron Selected data, in which the Cherenkov Detector read out a positive signal. Plot (c) shows the Electron Suppressed plots. This includes pions and protons and a few remanent electrons that were not detected by the Cherenkov Detector.

32

Figure 20: This plot shows 8 GeV Constrained Fit of the Electron Suppressed data set. In this data set there is no way to distinguish between the electron and pion peaks. Therefore the fits are nearly identical to the fits of the Electron Suppressed sample.

Beam Particle Composition at Different Momentum

After identifying the different peaks of the ToF data, I integrated under the gaussian curve of each best fit in order to calculate the number of particles in each peak. I was also able to calculate a systematic error associated with the integral and therefore an uncertainty in the beam composition.

The percent beam composition of the Test Beam changed as the beam momentum changed. At lower momentum the Test Beam was dominated by electrons, with very small contributions from protons and pions. As the momentum increased the concentration of pions and protons increased.

Table 7: Percent Beam Composition at Different Momentum

Momentum	Electrons	Pions	Protons	Unidentified
1.55 GeV	96.662 ± 0.003	0.692 ± 0.0003	0.3849 ± 0.0002	2.657 ± 0.0003
2 GeV	96.994 ± 0.003	1.034 ± 0.006	0.5124 ± 0.0002	1.4596 ± 0.0003
4 GeV	84.929 ± 0.002	11.794 ± 0.002	2.5071 ± 0.0004	0.7699 ± 0.0003
6 GeV	71.754 ± 0.002	23.443± 0.001	4.2682 ± 0.0007	0.5348 ± 0.0002
8 GeV	56.627 ± 0.001	35.188 ± 0.002	6.7145 ± 0.0006	1.4705 ± 0.0002

Cherenkov Efficiency

There are a certain number of electrons that do not trigger the Cherenkov detector in the Test Beam. In order to calculate the efficiency of the Cherenkov detector I compared the number of electrons in the Electron Suppressed data sample to the number of electrons in the entire data sample. I think calculated the error for the efficiency. It was only possible to calculate the efficiency for the 2 GeV and 1.55 GeV Test Beams because at higher momentum the pion peak and the electron peak became indistinguishable. The efficiency of the Cherenkov detector was used to separate the indistinguishable peaks from one another. The value used to separate the indistinguishable peaks was the average efficiency of the Cherenkov Detector,

which is $6.96 \times 10^{-4} \pm 0.84 \times 10^{-4}$.

$$\epsilon = \frac{N_{e-suppressed}}{N_{e-suppressed} + N_{e-selected}} \tag{7}$$

$$\sigma = \sqrt{\frac{\epsilon(\epsilon - 1)}{N_{e-suppressed} + N_{e-selected}}} \tag{8}$$

Table 8: Cherenkov Efficiency

Beam Momentum	Effeciency	Error
1.55 GeV	5.655e-4	8.335e-5
2 GeV	8.272e-4	8.483e-5

Data Acquisition (DAQ) Counter Offset

The estimated distance between the Upstream and Downstream counters is approximated to be 80 meters. However, when I entered in this value in order to calculated the expected ToF, the time values were consistently smaller than the times derived from the best fit of the data. I conducted a simple test to find more accurately the distance between the two counters. I entered in various distances into the calculations and compared the offsets for the proton peaks. I used the proton peaks because both the best fit of the electron and pion peaks differed much less dramatically from calculated expectations. The results from this exercise are shown on Table 9. In order to find the total deviation I found the sum of the differences between the measured proton ToF and the calculated ToF for each distance using the following equation.

$$\sum_{n=0}^{4} t_{measured} - t_{theoretical} \tag{9}$$

Table 9: ToF Comparisons At Various Distances Between Upstream and Downstream Counters

Momentum	Measured Proton ToF	Distance for Theoretical Calculations			
		85 meters	90 meters	100 meters	110 meters
1.55 GeV	51.83 ± 0.20	47.86	50.68	56.31	61.94
2 GeV	40.00 ± 0.14	29.62	31.36	34.85	38.34
4 GeV	7.947 ± 0.005	7.682	8.134	9.038	9.94
6 GeV	4.080 ± 0.003	3.435	3.637	4.041	4.44
8 GeV	2.439 ± 0.002	1.933	2.047	2.274	2.50
	Sum of Deviations	**15.75**	**10.43**	**-0.226**	**-10.87**

Timing Calibration of ToF System

The results of the Counter Offset analysis allowed for various conclusions about both the fits and the counting mechanism used by the ToF system. The 2 GeV proton peak that

was measured was consistently greater than the theoretical calculations. This is due to the systematic peak at 38 ns that is associated with the beam spill. This table suggests that the actual distance between the Upstream and Downstream counter is closer to 100 meters than 80 meters. A survey of the Test Beam concluded that the distance between the Upstream and Downstream counters was 104.5 meters. This is fairly consistent with the theoretical calculations which suggest the least deviations from the measure ToF occur at 100 meters.

The spill cycle of the proton beam used to produce the Test Beam is well known. A bunch of protons hits the target at 18.831 ns intervals. The systematic peaks seen on the plots are associated with these 18.831 ns intervals. I fit each of these peaks on the 4 GeV data set and derived the DAQ recorded time between each bunch of protons. These results can be seen on Table 10. I used the first peak of electrons, that was centered approximately around 0 ns, as the first systematic peak. The mean of best fit for the second peak is significantly lower than 18.831 ns, however this is possibly due to the time delay associated with starting the data acquisition after a trigger is received. The distance between first and second peaks as well as the difference between the second and third peaks are most useful because they are not affected by the time delay from the trigger. This difference is also significant. The results suggest that the DAQ counter is not actually counting time accurately.

Table 10: Analysis of Accidental Peaks for 4 GeV Test Beam Momentum

Expected	Peak Number	Mean of Best Fit	Difference of Consecutive Peaks	Period Ratio
0 ns	0	-0.01±0.002		
18.831 ns	1	17.69±0.14	17.70±0.16	0.939± 0.021
18.831 ns	2	35.82±0.05	18.13±0.14	0.959± 0.008
18.831 ns	3	53.85±0.06	18.03±0.08	0.954± 0.004

These systematic offsets of the DAQ counter allowed for a calibration of the ToF data. The average of the ToF of the systematic peaks was 17.953 ± 0.019 ns. The ratio of this to the actual ToF for the systematic peaks to the average derived from the fits was A = 1.049

± 0.001. This value for A was used to calibrate the ToF times.

$$\Delta t = t_{calibrated} - t_{theoretical} \tag{10}$$

$$t_{calibrated} = t_{measured} \times A \tag{11}$$

Time of Flight Comparisons

The measured ToF for the protons based on the the gaussian fit was almost always con-sistently larger than the expected ToF. The measured ToF for the pions was only slightly larger than the expected value at low momentum, 1.55 GeV and 2 GeV. However at higher momentum there is a larger difference between the expected and measured value. This could be because at higher momentum the pion and electron peaks merge together. This makes it difficult to correctly measure the mean of the gaussians. In order to better distinguish, I first fit the electron peak in the electron selected data set, then used the same parameters to fit the combined data set.

Table 11: ToF Comparisons Calculated vs Mean form Gaussian Best Fit

Momentum	Particle	Expected ToF (ns)	Calibrated ToF (ns) $\pm$ Error	Sigma $\sigma \pm$ Error
1.55 GeV	proton	56.31	54.37 $\pm$ 0.20	2.33 $\pm$ 0.25
	pion	1.33	1.14 $\pm$ 0.013	0.27 $\pm$ 0.01
	electron	-0.0101	-0.115 $\pm$ 0.00093	0.26 $\pm$ 0.0008
2 GeV	proton	34.85	41.96 $\pm$ 0.14	2.52 $\pm$ 0.21
	pion	0.801	0.921 $\pm$ 0.006	0.22 $\pm$ 0.005
	electron	-0.0102	-0.076 $\pm$ 0.0006	0.22 $\pm$ 0.0005
4 GeV	proton	9.04	8.336 $\pm$ 0.005	0.336 $\pm$ 0.004
	pion	0.193	0.211 $\pm$ 0.0014	0.199 $\pm$ 0.001
	electron	-0.0102	0.0108$\pm$ 0.0005	0.199 $\pm$ 0.004
6 GeV	proton	4.041	4.27 $\pm$ 0.003	0.273 $\pm$ 0.002
	pion	0.0800	0.138$\pm$ 0.008	0.547$\pm$ 0.003
	electron	-0.0102	0.0732 $\pm$ 0.005	0.629 $\pm$ 0.006
8 GeV	proton	2.275	2.559 $\pm$ 0.002	0.231$\pm$ 0.001
	pion	0.0406	0.142 $\pm$ 0.001	0.221 $\pm$ 0.0007
	electron	-0.0102	0.0741 $\pm$ 0.0006	0.221 $\pm$ 0.0005

Conclusion

Last semester I concluded that the geometries in the Neutrinos in the Main Injector Beam simulation were correct. This semester I calibrated the Time of Flight data for electrons, pions and protons. The calculated versus measure ToF data can be seen on Table 9. By fitting a gaussian to the ToF data for the 120 GeV protons I derived a timing resolution of $\sigma = 0.2319 \pm 0.0006$ ns. I concluded that the average efficiency of the Cherenkov Detector was $6.96 \times 10^{-4} \pm 0.84 \times 10^{-4}$. I found that the beam composition changed as the momentum changed. Consistently the number of electrons decreased as beam momentum increased. The number of pions and protons increased as the beam momentum increased. My final conclusion was that the Data Acquisition system's timing counter for the ToF system is counting more quickly than it should be. The DAQ system records a nanosecond as approximately 0.954 ± 0.004 ns. The ratio of this to the actual ToF for the systematic peaks to the average derived from the fits was $A = 1.049 \pm 0.001$. This value for A was used to calibrate the ToF times.

Acknowledgements

I would like to thank Professor Jeff Nelson, my Research Advisor, for his extensive assistance and guidance through my senior thesis project this past year. I would also like to thank Anne Norrick, a graduate student working on MINERvA for all of her help in completing my research. I could not have completed this project without the support of the William and Mary Physics Department.

Works Cited

Aliaga, Leo. "MINERvA Neutrino Detector Response Measured with Test Beam Data." 7 Apr. 2015. Web. 21 Apr. 2015.

Bichsel, H., D. E. Groom, and S. R. Klein. "PASSAGE OF PARTICLES THROUGH MATTER: Multiple Scattering through Small Angles." 10 Jan. 2004. Web. 21 Apr. 2015.

Appendix

Upstream Time 120GeV Protons
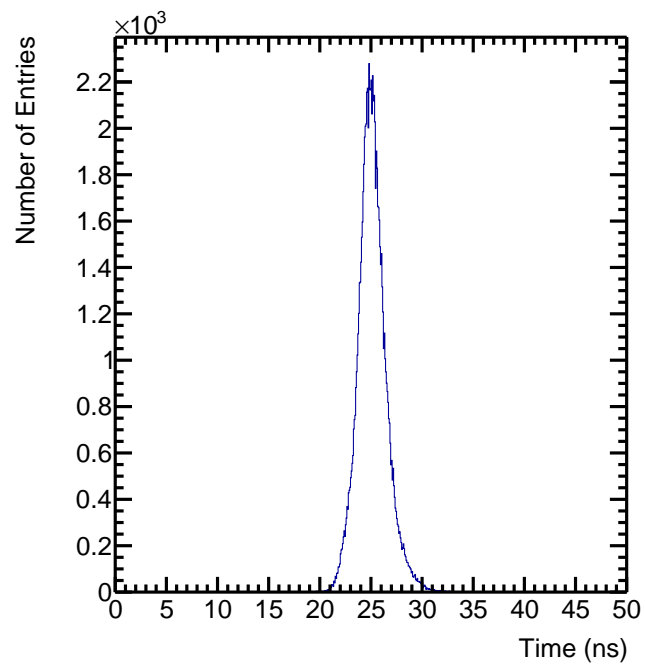
Downstream Time 120GeV Protons
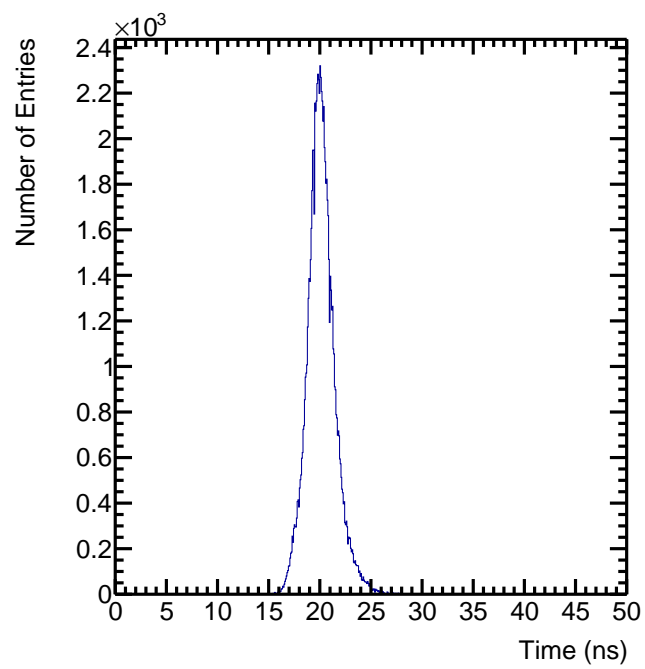
Time Difference 120GeV Protons
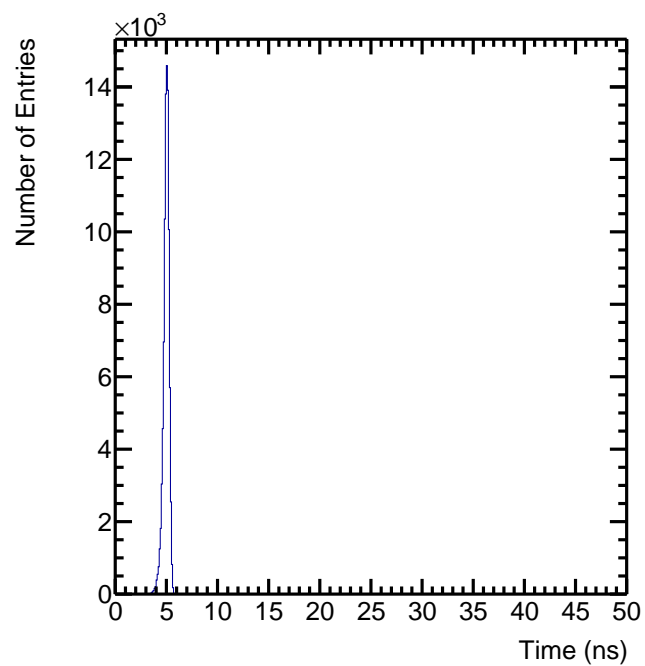
Time of Flight 120GeV Protons
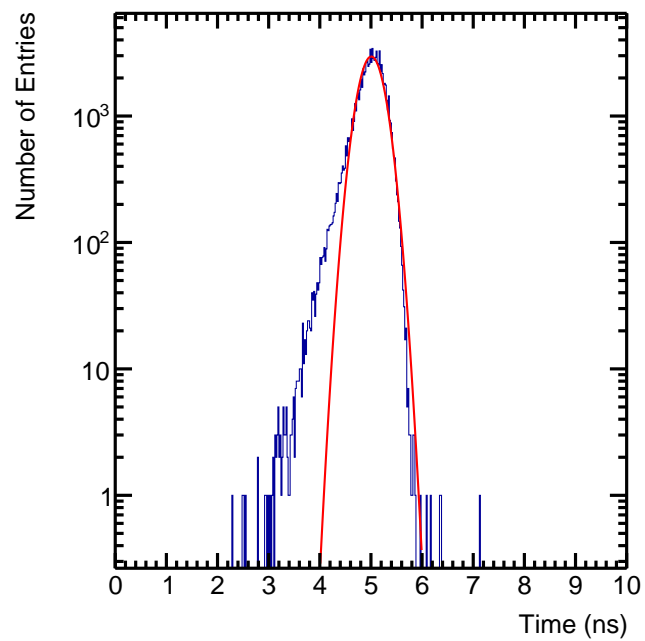
Upstream Time 1.55GeV
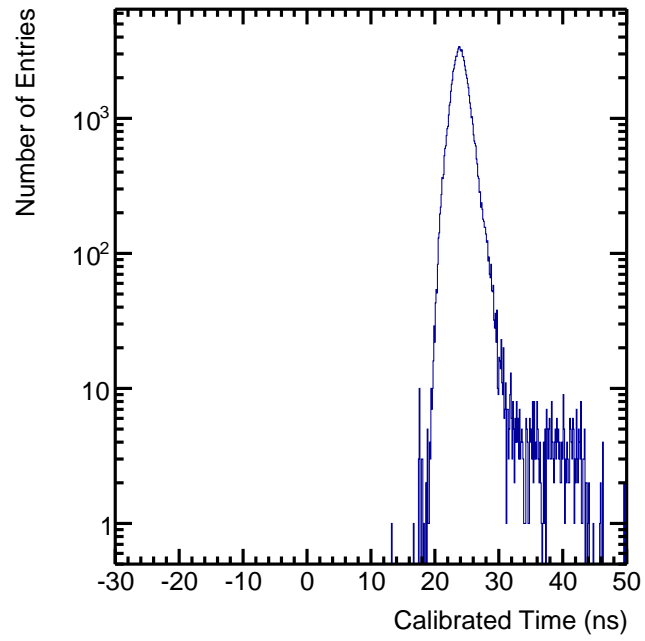
Downstream Time 1.55GeV
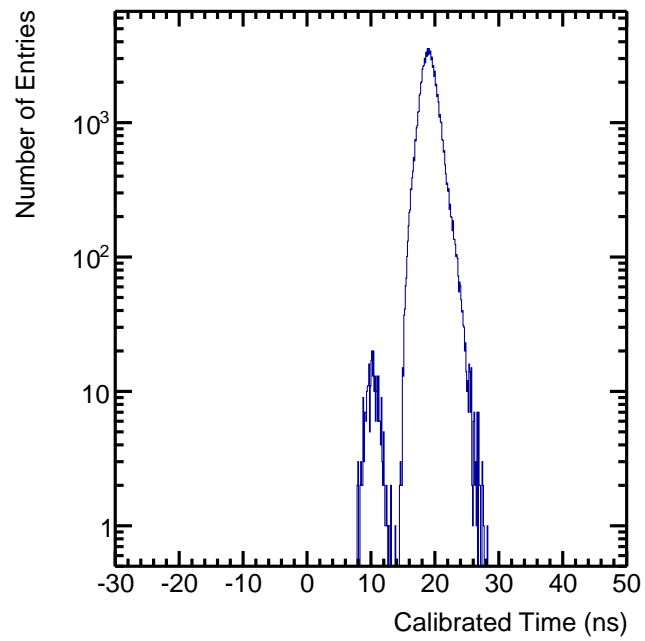
Time of Flight 1.55GeV Electron Suppressed
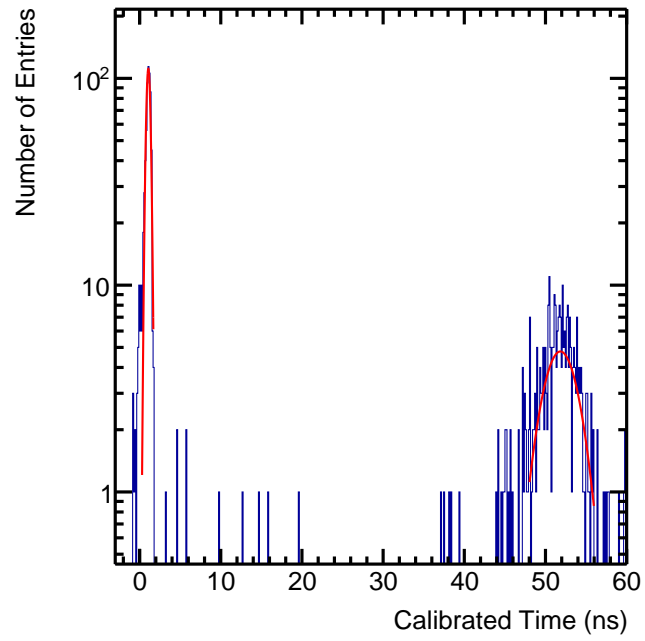
Time of Flight 1.55GeV Electron Selected
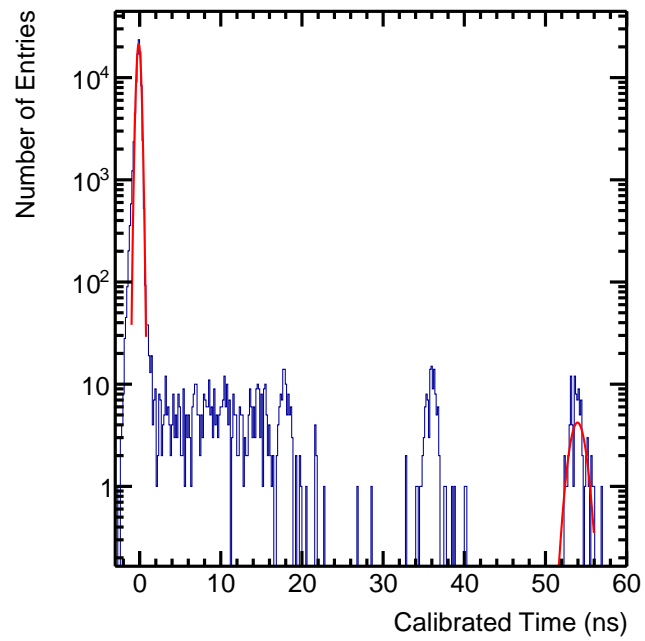
Time of Flight 1.55GeV Electron Selected Zoomed
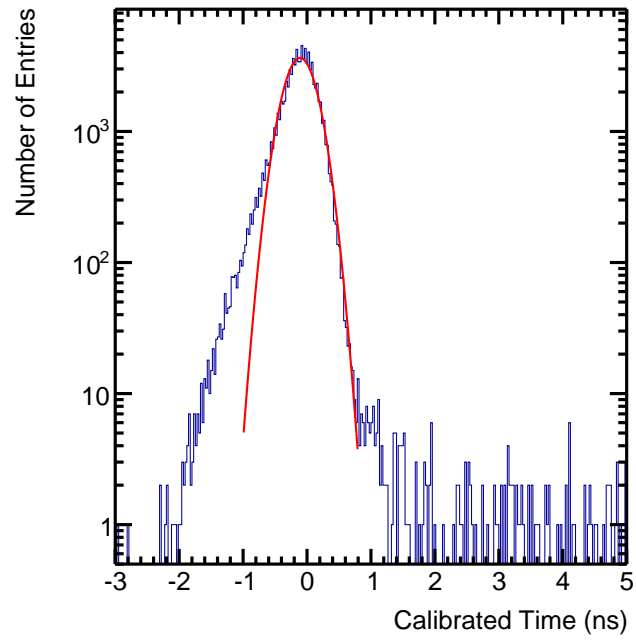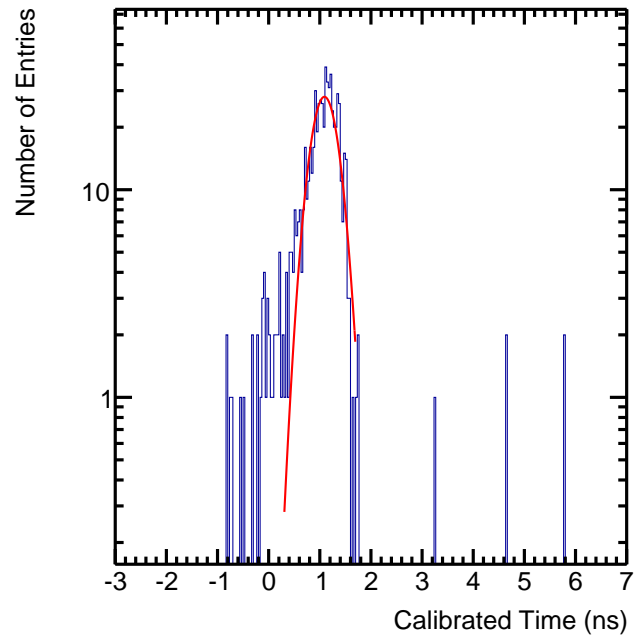
Time of Flight 1.55GeV Electron Suppressed Zoomed

Time of Flight 1.55GeV Combined

Time of Flight 1.55GeV Combined Constrained Fits
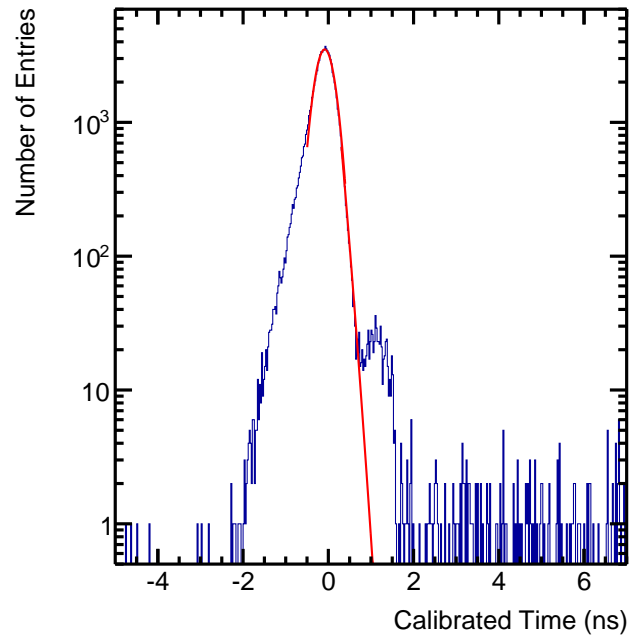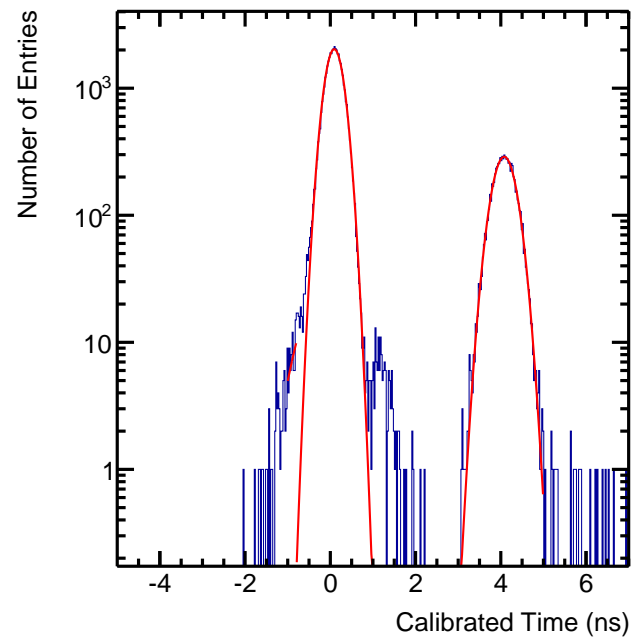

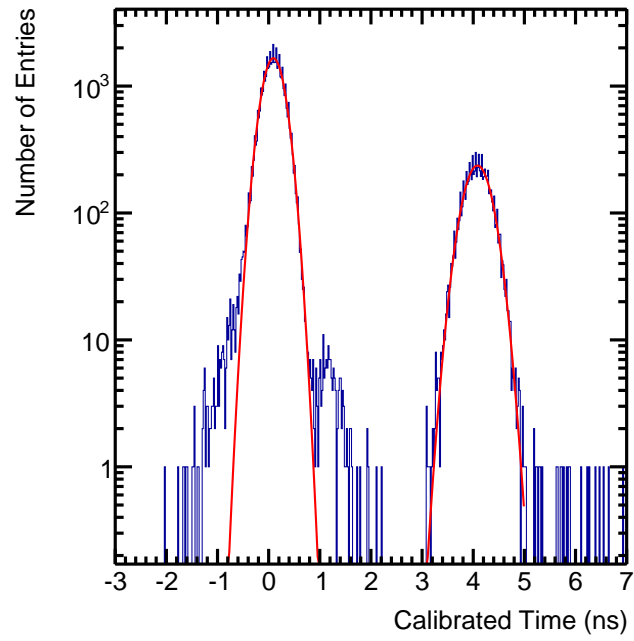Upstream Time 2GeV
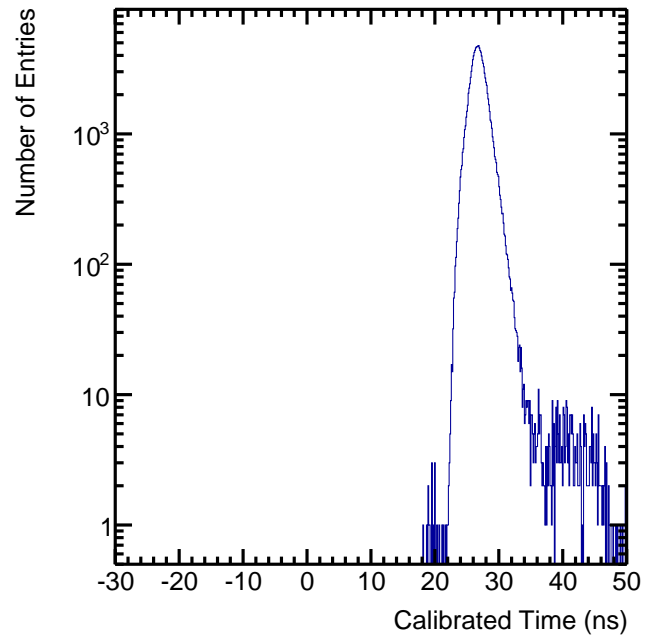
Downstream Time 2GeV
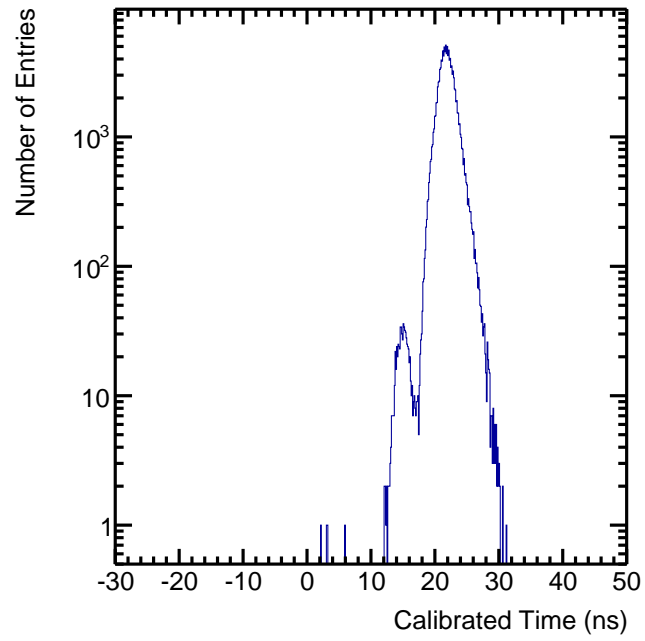
Time Difference 2GeV
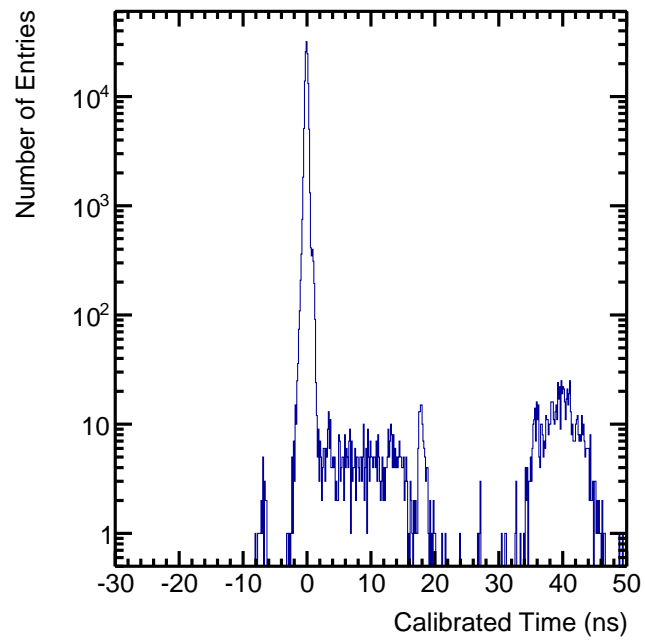
Time of Flight 2GeV Electron Suppressed
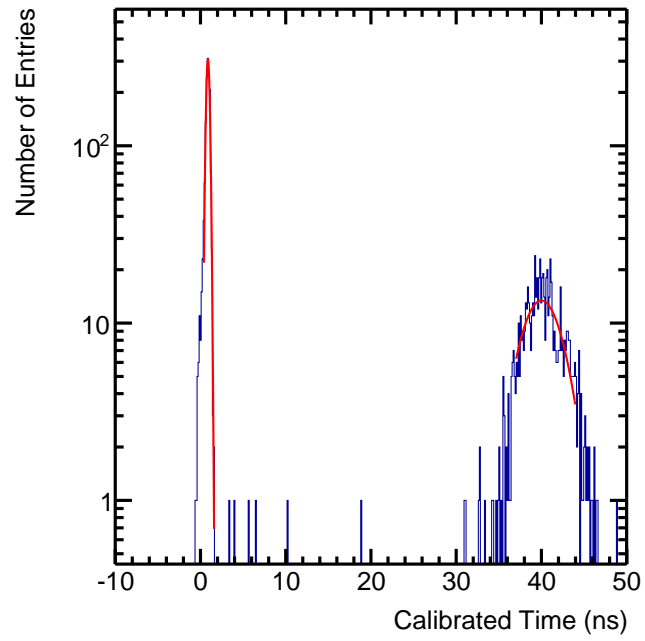
Time of Flight 2GeV Electron Selected
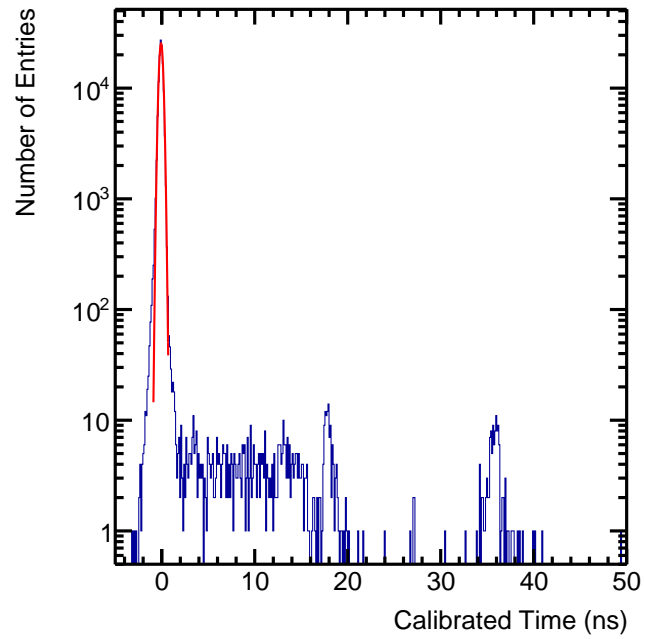
Time of Flight 2GeV Electron Selected Zoomed
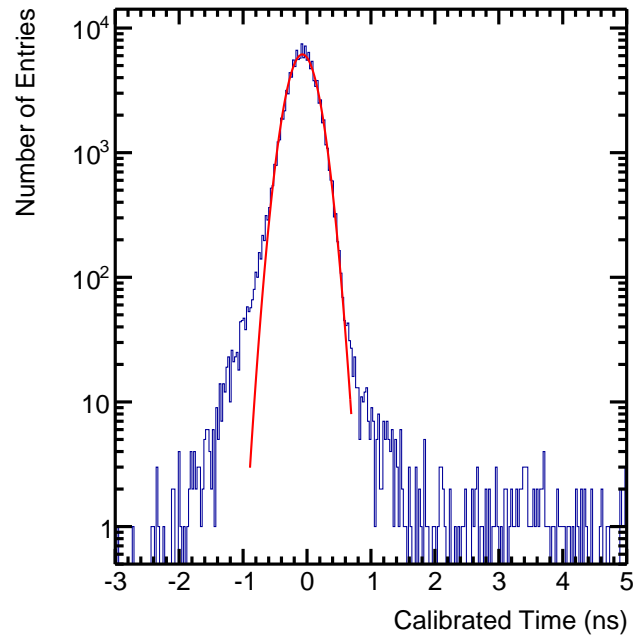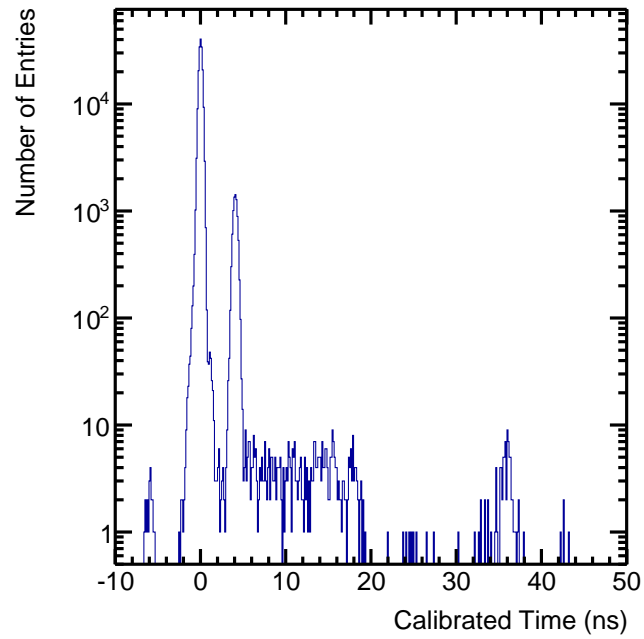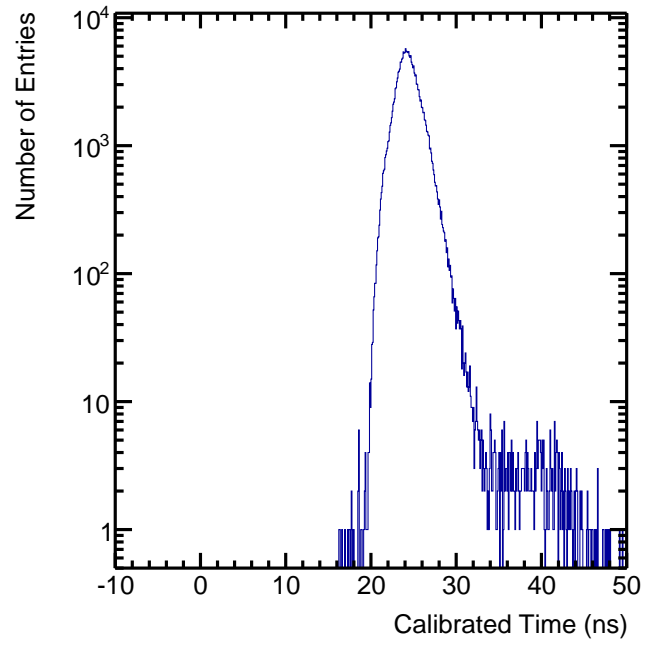

Time of Flight 2GeV Electron Suppressed Zoomed
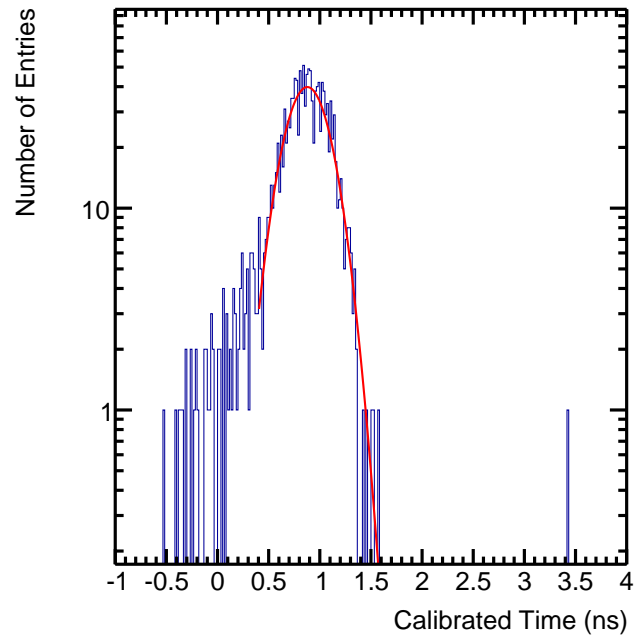
Time of Flight 2GeV Electron Suppressed Constrained Fit
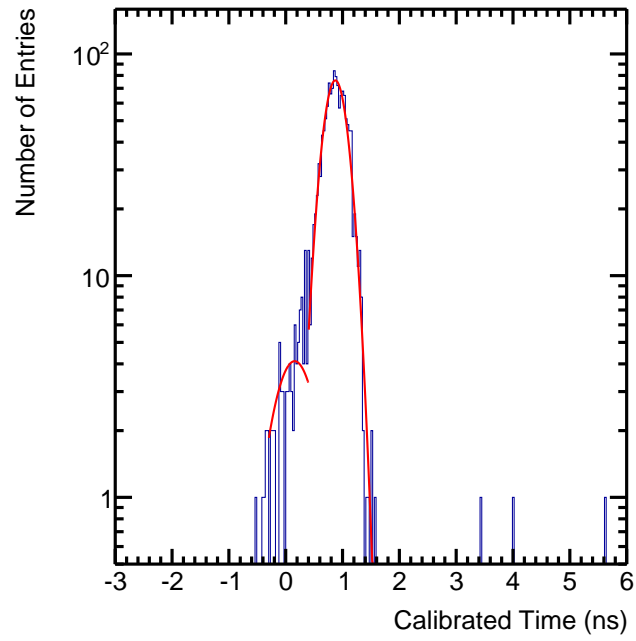
Time of Flight 2GeV Combined
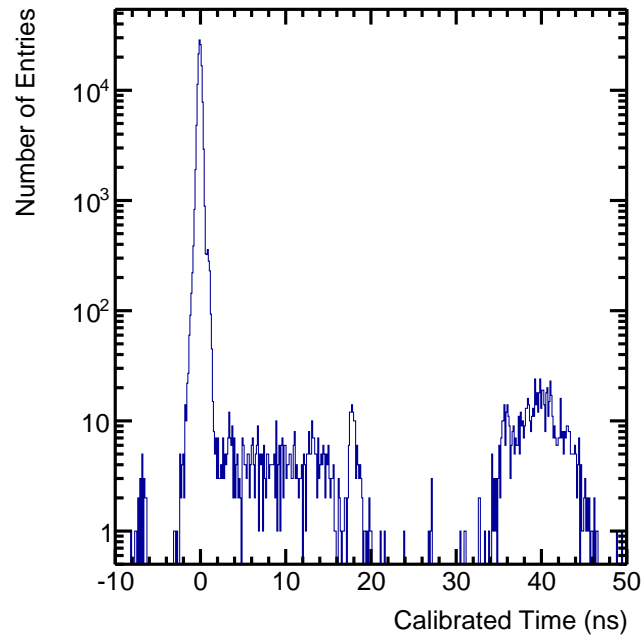
Time of Flight 2GeV Combined Constrained fit
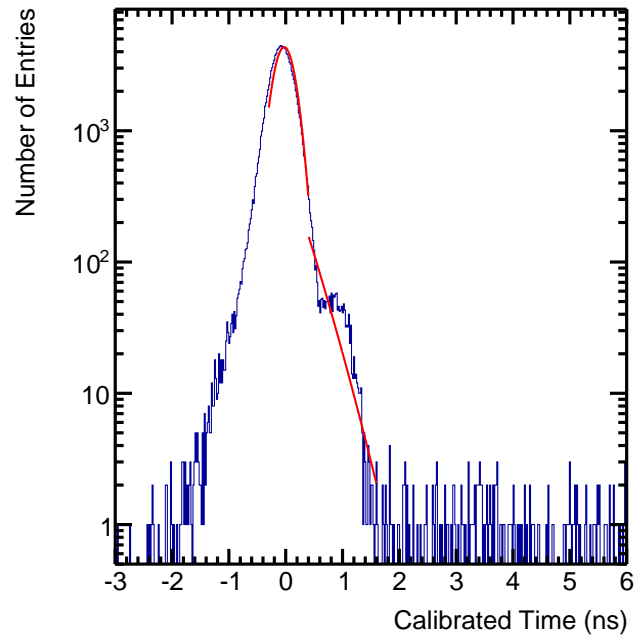
Upstream Time 4GeV
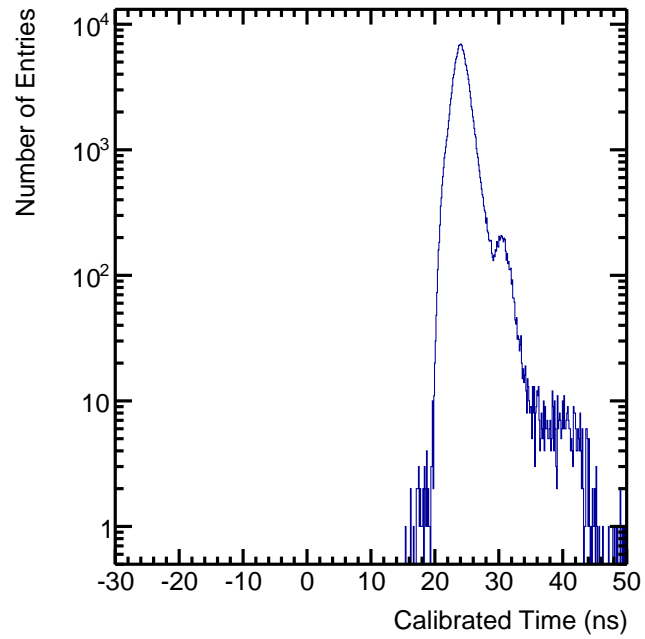
Downstream Time 4GeV
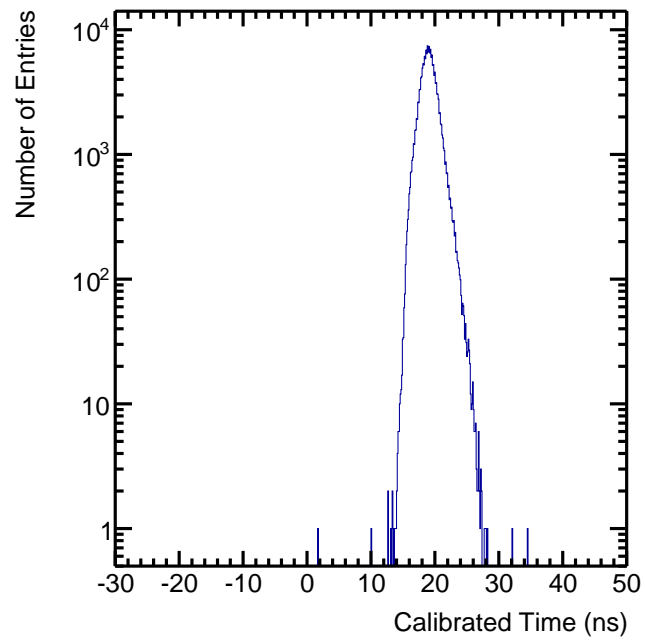
Time Difference 4GeV
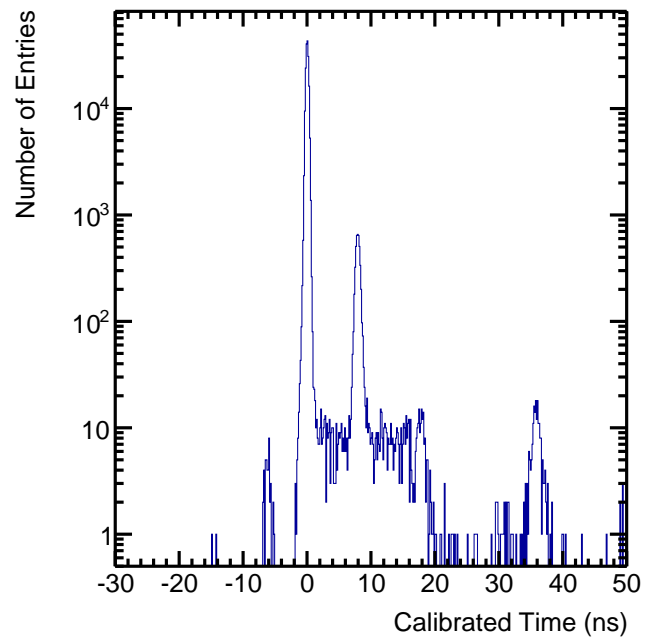
Time of Flight 4GeV Electron Selected
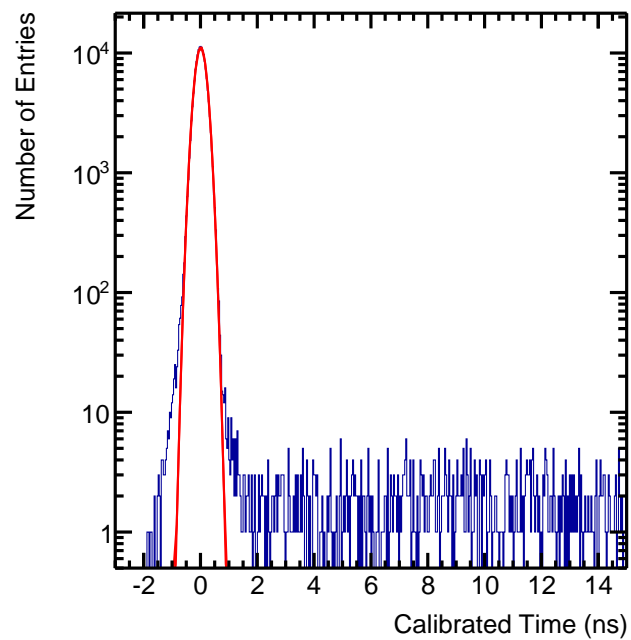
Time of Flight 4GeV Electron Suppressed
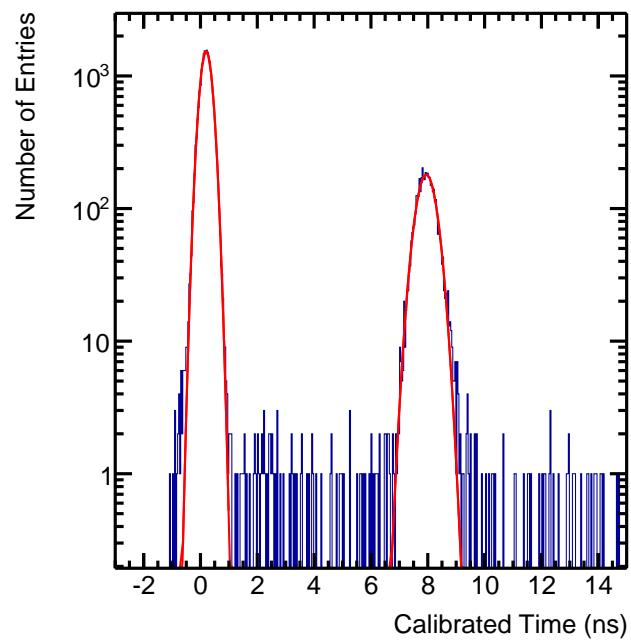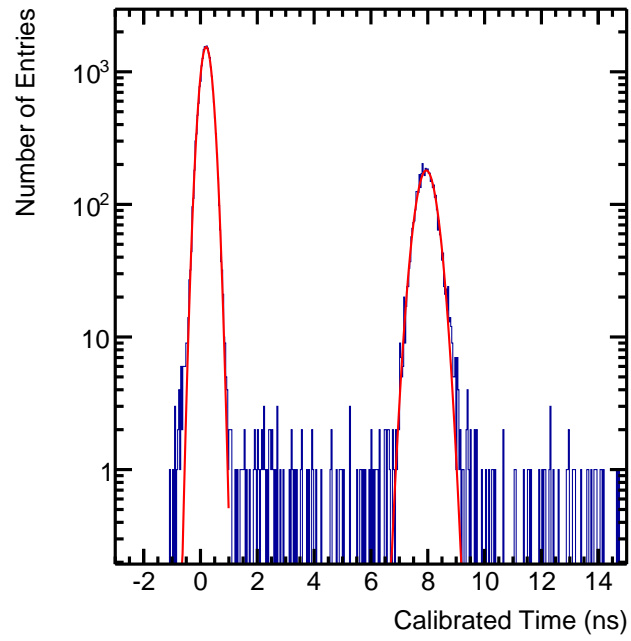
Time of Flight 4GeV Combined
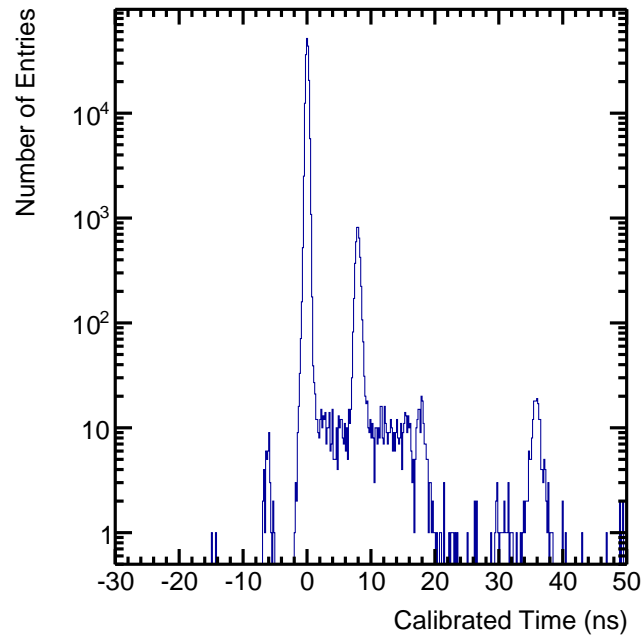
Time of Flight 4GeV Combined Constrained Fit
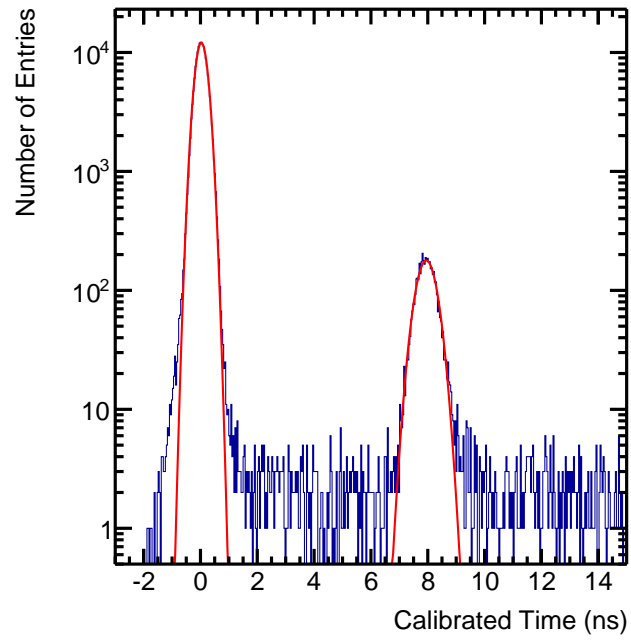
Upstream Time 6GeV
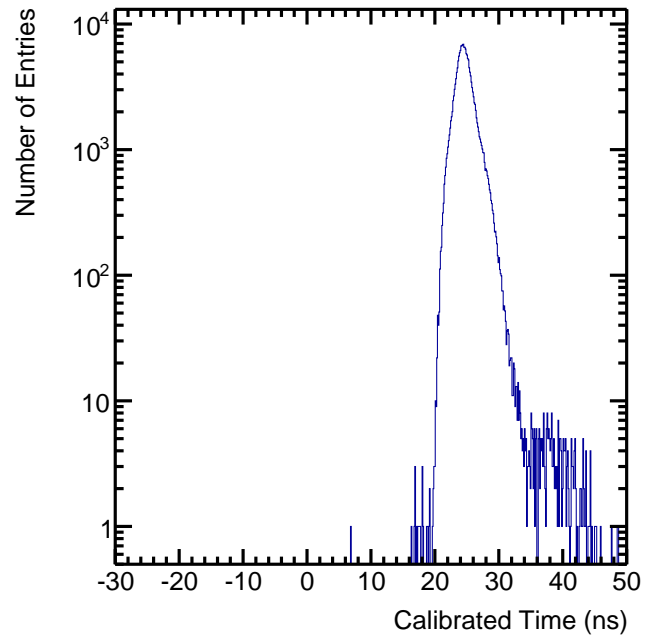
Downstream Time 6GeV
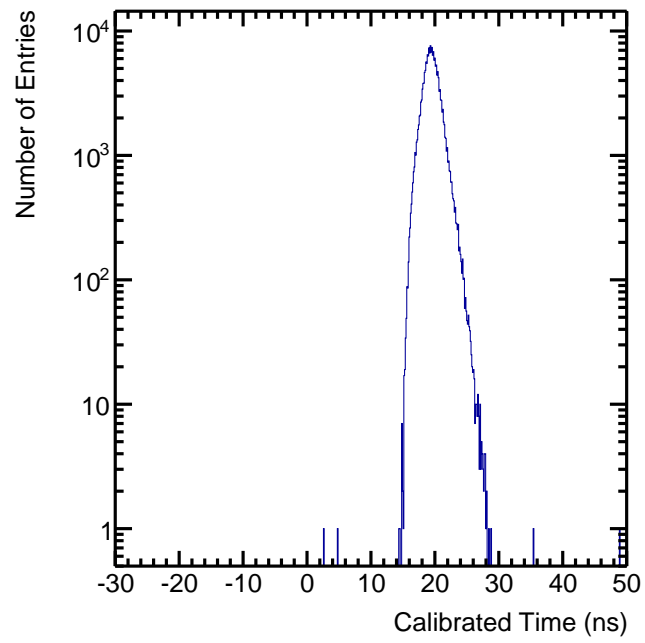
Time Difference 6GeV
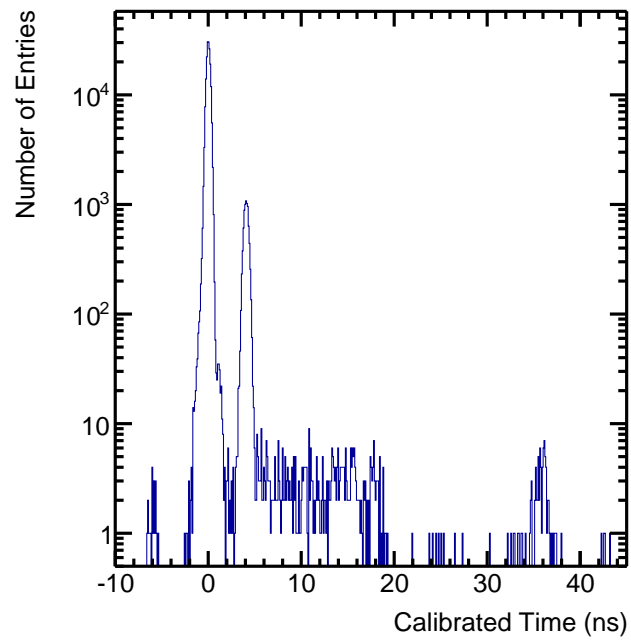
Time of Flight 6GeV Electron Selected
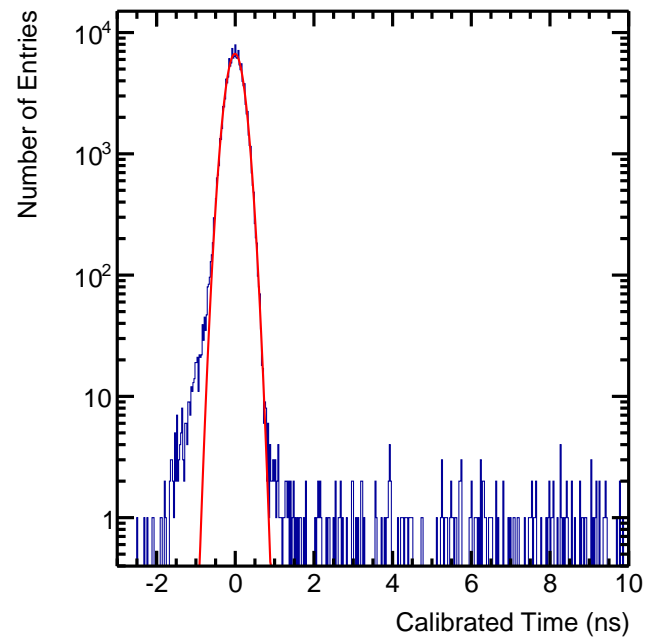
Time of Flight 6GeV Electron Suppressed

Time of Flight 6GeV Electron Suppressed Constrained Fit
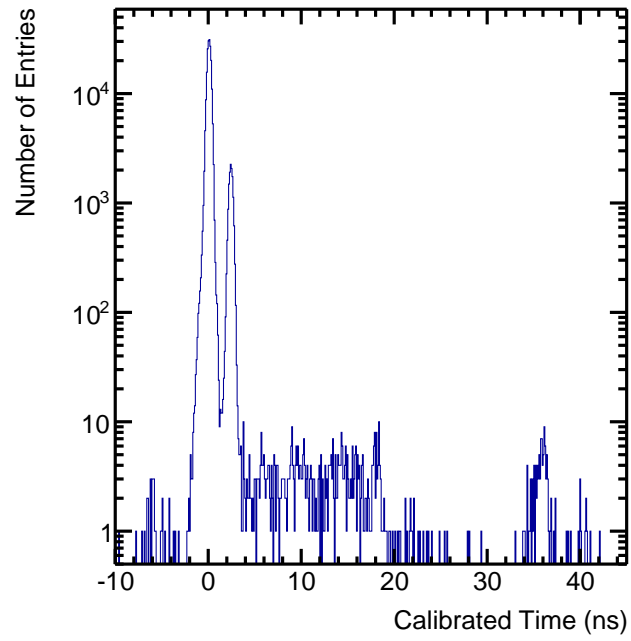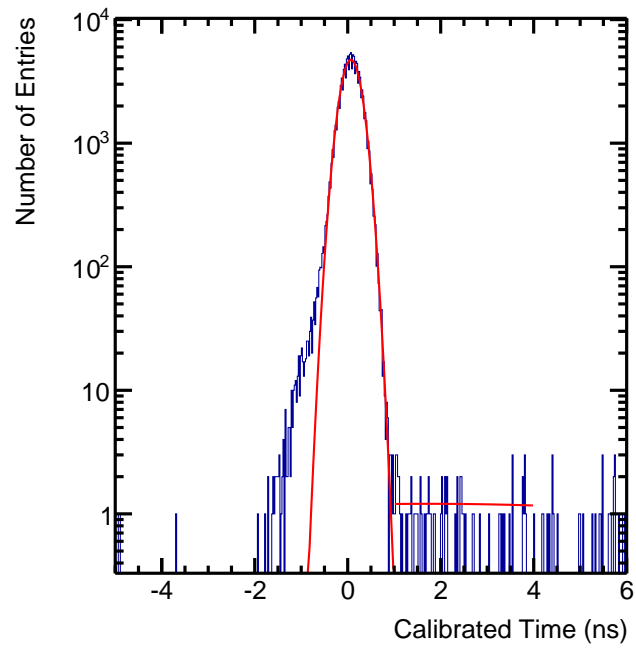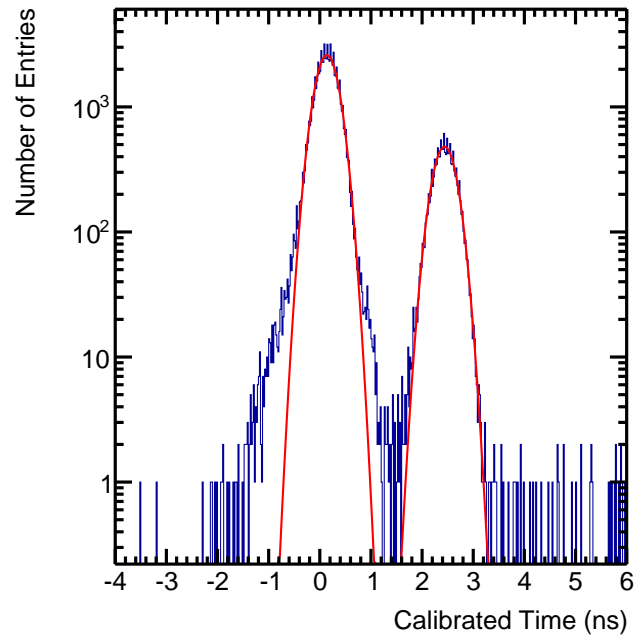

Time of Flight 6GeV Combined

Upstream Time 8GeV

Downstream Time 8GeV
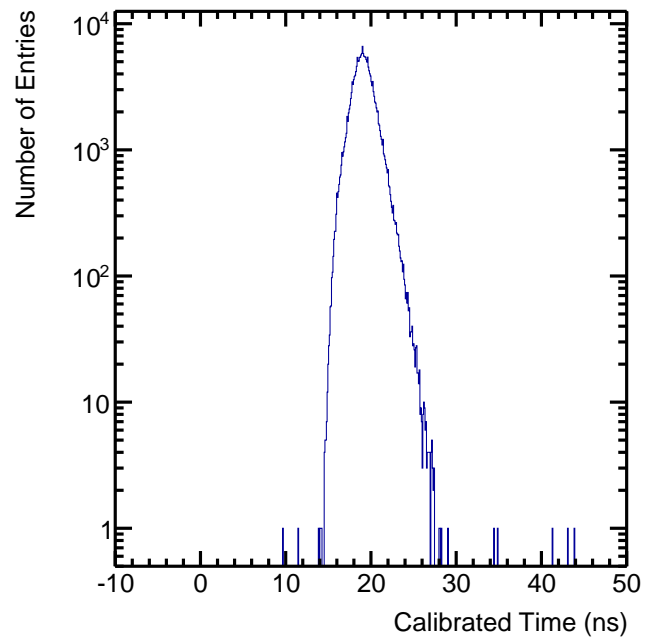
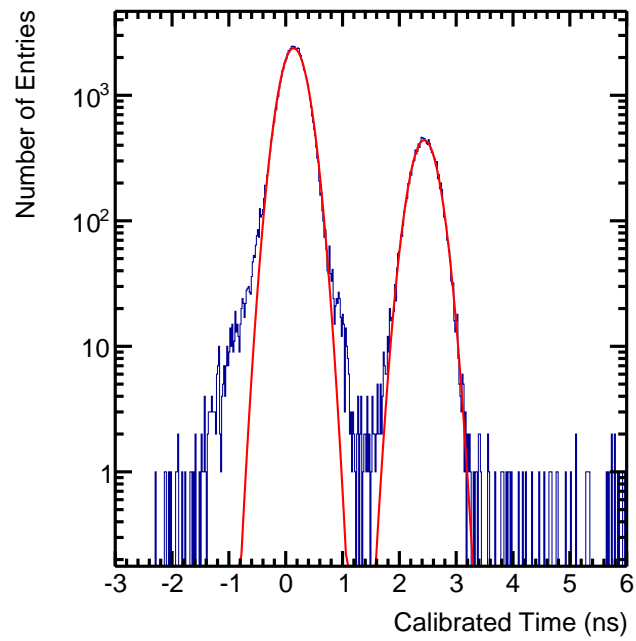## Time Difference 8GeV

Time of Flight 8GeV Electron Selected

Time of Flight 8GeV Electron Suppressed

Time of Flight 8GeV Electron Suppressed Constrained Fit

Time of Flight 8GeV Combined